Title: Intranasal self-amplifying RNA SARS-CoV-2 vaccine produces protective respiratory and systemic immunity and prevents viral transmission

Authors: Madeleine F. Jennewein[1†], Michael D. Schultz[2†], Samuel Beaver[1], Peter Battisti[1], Julie Bakken[1], Derek Hanson[1], Jobaida Akther[3], Raodoh Mohamath[1], Jasneet Singh[1], Noah Cross[1], Sierra Reed[1], Davies Kalange[3], Jeremy B. Foote[2], R. Glenn King[2], Aaron Silva-Sanchez[3], Davide Botta[2], Alana Gerhardt[1], Corey Casper[1,4,5,6], Troy D. Randall[3], Frances E. Lund[2], Emily A. Voigt[1*]

Affiliations:

[1]Access to Advanced Health Institute (formerly Infectious Disease Research Institute); Seattle, WA 98102, USA.

[2]Department of Microbiology, University of Alabama at Birmingham (UAB), Birmingham, AL 35294, USA

[3]Department of Medicine, Division of Clinical Immunology and Rheumatology, UAB, Birmingham, AL 35294, USA

[4]Department of Global Health, University of Washington; Seattle, WA 98195, USA.

[5]Department of Medicine, University of Washington; Seattle, WA 98195, USA.

[6]Vaccine and Infectious Disease Division, Fred Hutchinson Cancer Center; Seattle, WA 98109, USA.

†These authors contributed equally to this work.

*Corresponding author: emily.voigt@aahi.org

Short title: An intranasal saRNA vaccine for SARS-CoV-2

Abstract:

While mRNA vaccines have been effective in combating SARS-CoV-2, waning of vaccine-induced antibody responses and lack of vaccine-induced respiratory tract immunity contribute to ongoing infection and transmission. In this work, we compare and contrast intranasal (i.n.) and intramuscular (i.m.) administration of a SARS-CoV-2 self-amplifying RNA (saRNA) vaccine delivered by a nanostructured lipid carrier (NLC). Both i.m. and i.n. vaccines induce potent systemic serum neutralizing antibodies, bone marrow-resident IgG-secreting cells, and robust lymphoid tissue T cell immune responses. The i.n. vaccine additionally induces robust respiratory mucosal immune responses, including SARS-CoV-2-reactive lung-resident memory and lung-homing T cell populations. As a booster following previous i.m. vaccination, the i.n. vaccine also elicits the development of mucosal virus-specific T cells. Both the i.m. and i.n. administered vaccines protect hamsters from infection-associated morbidity upon viral challenge, significantly reducing viral loads and preventing challenged hamsters from transmitting virus to naive cagemates. This saRNA vaccine's potent systemic immunogenicity, and additional mucosal immunogenicity when delivered i.n., may be key for combating SARS-CoV-2 and other respiratory pathogens.

One Sentence Summary:

Intranasal SARS-CoV-2 saRNA vaccination induces systemic and mucosal immunity in mice, and prevents morbidity and blocks viral transmission in hamsters.

46 **Main Text:**

47 **INTRODUCTION**

48 The ongoing severe acute respiratory syndrome coronavirus 2 (SARS-CoV-2) pandemic has led
49 to the rapid advancement and development of novel vaccines for coronavirus disease 2019
50 (COVID-19). Since their introduction in late 2020, two now FDA-approved mRNA vaccines
51 (Comirnaty and Spikevax) have had a remarkable impact on the trajectory of the pandemic and
52 were developed at unprecedented speeds (*1*). However, while these vaccines have displayed
53 remarkable efficacy at preventing severe COVID-19 and slowing the worldwide pandemic, the
54 lack of vaccine-induced local immunity in the respiratory tract allows for mild infection of
55 vaccinated individuals, resulting in transmission of the virus, despite prior vaccination (*2–4*).
56 Between lack of vaccine induction of mucosal immunity, newly emerging variants (*5*), waning
57 efficacy of currently approved mRNA vaccines (*6*), need for frequent booster doses (*7*), vaccine
58 hesitancy in part fueled by a fear of needles (*8*), and limited access to cold chain storage (*9*),
59 global susceptibility to SARS-CoV-2 remains high. Improved vaccines and associated
60 technologies are therefore necessary to fully combat the epidemic.

61

62 We previously developed an intramuscularly (i.m.) administered nanostructured lipid carrier
63 (NLC)-delivered self-amplifying RNA (saRNA) vaccine against SARS-CoV-2 (*10*, *11*), which
64 induces both high serum neutralizing responses (*12–14*) and robust activation of systemic $CD4^+$
65 and $CD8^+$ T cells, responses that may be critical to sustained potent immunity (*13*). This saRNA-
66 NLC vaccine platform additionally has unique thermostability relative to other mRNA delivery
67 systems (*11*, *15–17*), as it may be readily lyophilized and stored at room temperature for months
68 or under refrigeration likely for years (*11*, *17*).

However, we wanted to examine the potential for this vaccine to be administered intranasally (i.n.) to stimulate mucosal immune responses (*18*), which may be key to improving sustained, potent immunity to SARS-CoV-2 and other respiratory pathogens. Unlike i.m. administered vaccines, i.n. vaccines induce critical immune cells within the mucosa and respiratory tract, generating IgA-secreting cells as well as specific effector cell subsets, including tissue-resident memory (T_{RM}) T cells that are maintained within the lung (*19–26*). Such mucosal immunity, mediated by IgA antibodies and lung-resident memory T and B cells (*27*), can prevent early-stage infection and viral replication and shedding, minimizing chances for viral transmission (*20*, *21*, *26*, *28*, *29*). Effective i.n. vaccines can also induce cross-reactive antibodies and thus provide expanded protection to multiple strains (*30*). Intranasal vaccination also presents many other advantages, such as easier needle-free administration, higher patient compliance, simpler pediatric dosing, and easier storage and transport (*31*), and thus potentially increased vaccine uptake. However, while several i.n. vaccines are currently under development for SARS-CoV-2, most of these rely on older vaccine technologies, i.e., live-attenuated viruses and viral vectors (*1*), creating a slow pathway to manufacturing, testing, and licensing. Fortunately, bridging RNA vaccine technologies to i.n. delivery is possible, combining the production speed of RNA vaccines with the mucosal immune stimulation of i.n. vaccines.

We now demonstrate that both i.n. and i.m. administrations of our saRNA SARS-CoV-2 vaccine strongly induce systemic immunity in preclinical models and prevent viral transmission by vaccinated, virally challenged hamsters. Intranasal dosing uniquely induces strong mucosal T cell immunity, and a heterologous dosing strategy—i.m. prime followed by i.n. boosting—

92 appears to show the greatest potential to maximize mucosal and systemic immunity, leading to
93 prevention of viral transmission. This saRNA-NLC vaccine candidate combines the flexibility
94 and manufacturability of RNA vaccines with potent induction of mucosal immunity using a
95 thermostable formulation that represents a significant new tool for current and future pandemic
96 responses.
97
98 **RESULTS**
99

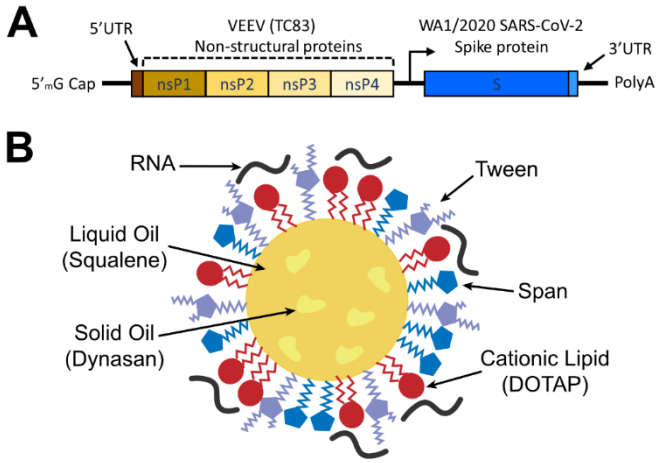

100
101 **Fig. 1. Design of saRNA-NLC SARS-CoV-2 vaccine AAHI-SC2**. **(A)** saRNA SARS-CoV-2
102 construct diagram. **(B)** NLC-RNA complex diagram.
103

104 *Intranasal saRNA-NLC vaccine stimulates robust systemic immune responses*

105 For development of an intranasally delivered saRNA vaccine against SARS-CoV-2, we
106 harnessed our previously developed and published long-term thermostable SARS-CoV-2
107 saRNA-NLC vaccine (*11*). This vaccine, currently in clinical trials using intramuscularly
108 administered material, contains a codon-optimized Wuhan-strain D614G SARS-CoV-2 spike
109 protein sequence driven by a Venezuelan equine encephalitis virus (VEEV)-based replicon
110 (Figure 1A) (*11*). This saRNA is complexed to the exterior of AAHI's proprietary NLC
111 nanoparticle to create the final vaccine product AAHI-SC2 (Figure 1B).

112

113 To investigate the ability of the saRNA-NLC vaccine to generate effective immunogenicity when
114 delivered intranasally, 6–8-week-old C57BL/6J mice were given prime and boost vaccine doses
115 of 1, 5, or 10 µg, 3 weeks apart. Control mice were i.n. dosed with 10 µg of a non-immunogenic
116 saRNA-NLC expressing the reporter protein secreted alkaline phosphatase 2 (SEAP). Systemic
117 immunogenicity was compared between groups. Serum, bone marrow, lung, and spleen tissues
118 were harvested after vaccination and tested for humoral (serum IgG and pseudovirus
119 neutralization titers; bone marrow antibody-secreting cells [ASCs] by enzyme-linked
120 immunospot [ELISpot]) and cellular (systemic T cell responses by intracellular cytokine staining
121 and flow cytometry [ICS-flow] and T cell ELISpot of splenocytes; mucosal T cell responses by
122 ICS-flow of lungs) vaccine-induced SARS-CoV-2-directed immune responses.

123

124 The i.n. saRNA-NLC vaccine elicited high serum spike-specific IgG and SARS-CoV-2 Wuhan-
125 strain neutralization titers that would be predicted to be protective (>1000 IC_{50}) (*32*, *33*) at all i.n.
126 doses after prime and boost (Figure 2A, B). Strikingly, at the 5 and10-µg doses, no significant

127 differences were observed between i.n. and i.m. vaccines post-boost, suggesting equivalent
128 induction of serum responses – the key correlates of protection for SARS-CoV-2 (*32*, *33*) – by
129 the i.n. vaccine. IgG1 and IgG2a serum antibody titers indicated that i.n. vaccination with the
130 saRNA-NLC vaccine maintains the desired Th1 bias seen with our i.m. vaccine (Figure 2C).
131 Next, bone marrow-resident ASCs were assessed post-boost by ELISpot to determine if there
132 was establishment of a memory niche for IgG-secreting ASCs. No differences were seen
133 between the i.n. and i.m. vaccines at either the 5- or 10-µg dose i.n. as compared to the 10-µg
134 dose i.m. (Figure 2D), further suggesting effective systemic induction by both delivery routes
135 and suggesting durability of response established by both vaccines.
136
137 Cell-mediated immunity, particularly T cell immunity, is also thought to be critical to sustained,
138 long-term protection against SARS-CoV-2 (*13*, *33*). We therefore investigated systemic cellular
139 responses in i.n. and i.m. vaccinated mouse spleens after boost, both by ELISpot and ICS.
140 Significant populations of IFNγ-secreting T cells were observed in both the i.n. and i.m. dosed
141 (10-µg dose) mouse groups as measured by ELISpot (Figure 2E), indicating effective induction
142 of effector T cells primed to respond to SARS-CoV-2. While the cell numbers were significantly
143 higher in the i.m. dosed group, both groups showed robust T cell responses. IL-5- and IL-17-
144 secreting cells were seen at negligible populations in either group (Figure 2F-G), suggesting a
145 strong Th1-biased response (*34*, *35*) induced by both the i.n. and i.m. vaccines with very little
146 induction of a potentially harmful Th2 response associated with immunopathology and natural
147 infection (*34*, *36*, *37*).
148

149 These robust, strongly Th1-skewed systemic $CD4^+$ and $CD8^+$ T cell responses were verified
150 using ICS-flow performed on mouse splenocytes collected post-vaccination. After prime-boost
151 immunization, significant populations of spike-reactive polyfunctional ($IFN\gamma^+$, $IL\text{-}2^+$, and
152 $TNF\alpha^+$) $CD8^+$ and $CD4^+$ T cells were observed in mice immunized with the 5- and 10-µg i.n.
153 vaccine doses and the 10-µg i.m. dose (Figure 2H, I), demonstrating strong T cell-mediated
154 responses induced by both i.m. and i.n. vaccines. The spike-reactive polyfunctional T cell
155 populations of $CD4^+$ T cells induced by the i.n. vaccine were lower than those induced by the
156 i.m. vaccine (20-30% reduction between the i.n. and i.m. vaccines at a 10-µg dose, $p = 0.0191$);
157 however, spike-reactive polyfunctional $CD8^+$ T cell populations were not significantly different
158 between the i.n. and i.m. vaccinated mice, and $CD4^+$ T cell responses induced by the i.n. vaccine
159 were still high, demonstrating effective seeding of systemic T cell immunity across all i.n. and
160 i.m. vaccinated mice. As seen with vaccine-induced antibody titers, a stronger induction of a
161 Th1-specific response (secretion of $IFN\gamma^+$, $IL\text{-}2^+$, or $TNF\alpha^+$) compared to a Th2 response
162 (secretion of $IL\text{-}5^+$ or $IL\text{-}10^+$) or a Th17 response (secretion of $IL\text{-}17^+$) occurred within the T cell
163 compartment in both i.n. and i.m. vaccinated mice and across all doses (Figure S2A), suggesting
164 an overall systemic functional response to the virus. These data therefore indicate that the i.n.
165 saRNA-NLC vaccine elicits humoral and cellular responses at levels predicted to be protective.
166

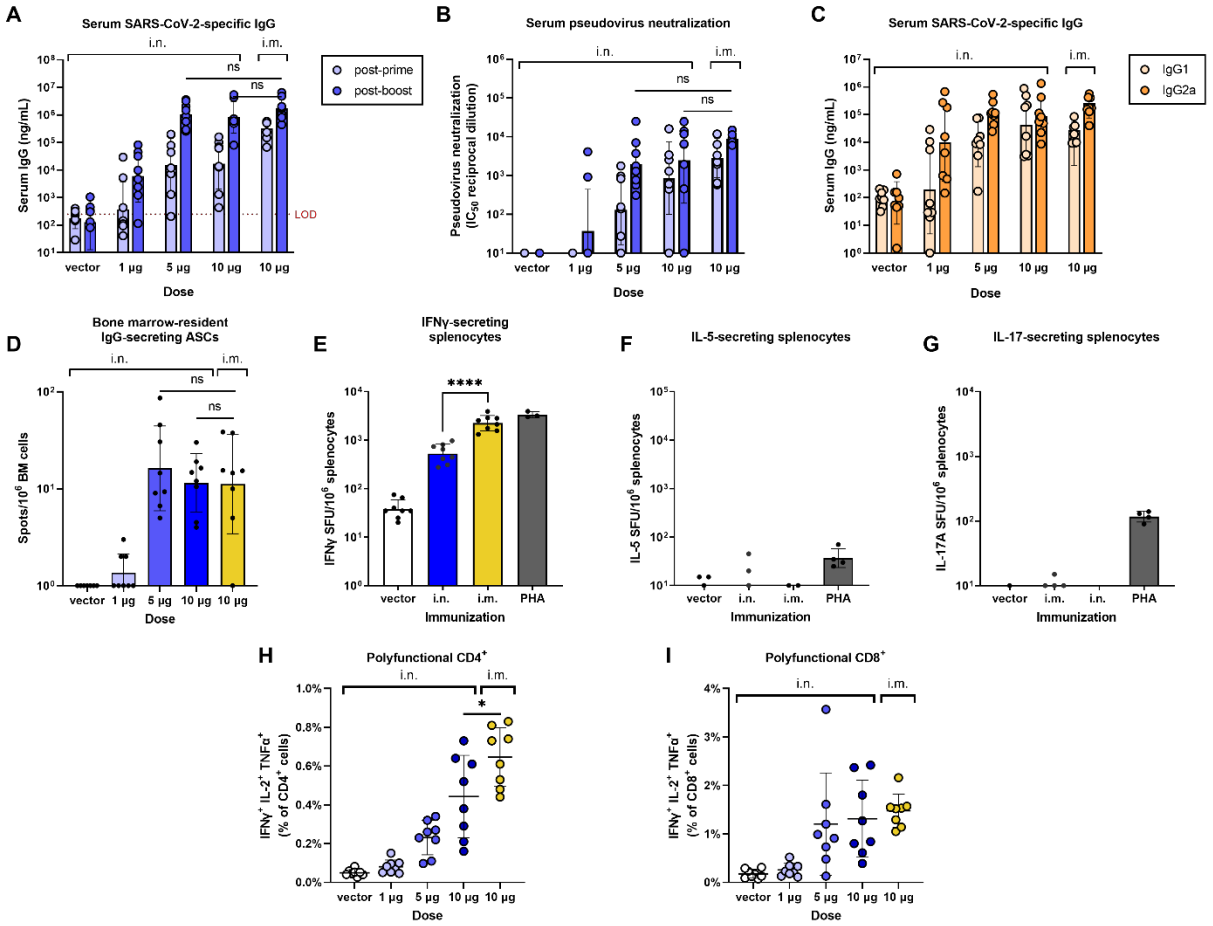

Fig. 2. Systemic immunogenicity of intranasally administered SARS-CoV-2 saRNA-NLC vaccine. Systemic immunogenicity was assessed 3 weeks post-prime or post-boost in C57BL/6J mice immunized with AAHI-SC2 i.m. at 10 µg or i.n. at 1, 5, or 10 µg or a vector control (SEAP) i.n. at 10 µg at day 0 and day 21. n = 8 mice per group, evenly split male-female. **(A)** Serum SARS-CoV-2 spike-specific IgG responses measured post-prime and post-boost. LOD = limit of detection. **(B)** Serum SARS-CoV-2 spike Wuhan pseudovirus neutralizing titers measured post-prime and post-boost. **(A-B)** Data were log transformed and analyzed by a mixed-effects model with Tukey's multiple comparisons test. **(C)** Serum spike-specific IgG1 and IgG2a responses measured post-boost. **(D)** Induction of bone marrow-resident spike-specific IgG-secreting ASCs as measured by ELISpot 3 weeks post-boost. **(E-G)** SARS-CoV-2 spike-

178 responsive secretion of IFNγ, IL-5, or IL-17a by splenocytes post-boost as measured by ELISpot
179 in mice dosed with 10 μg of saRNA. All bars on graphs show geometric mean ± geometric SD.
180 **(H-I)** Splenic spike-responsive polyfunctional T cells ($IFN\gamma^+$, $IL\text{-}2^+$, and $TNF\alpha^+$ $CD4^+$ or $CD8^+$
181 T cells) post-boost as measured by intracellular cytokine staining and flow cytometry. Horizontal
182 lines show mean ± SD. See Figure S1 for flow cytometry gating strategies. **(D-I)** Data were
183 analyzed by one-way ANOVA with Tukey's multiple comparisons test. *$p < 0.05$ and ****$p <$
184 0.0001.
185

186 *Intranasal vaccine administration induces specialized lung T cell populations*

187 While both i.m. and i.n. vaccines induce excellent systemic immunity, a key objective to
188 assessing i.n. immunization was to determine whether effective mucosal responses could be
189 generated with i.n. administration of an RNA vaccine. To that end, the lung T cell compartment
190 was analyzed from C57BL/6J mice vaccinated i.n. or i.m. with 10 µg of AAHI-SC2 3 weeks
191 post-prime and 3 weeks post-boost; the lung T cell compartment was analyzed by ICS-flow for
192 the presence of specialized T cell subsets that would indicate the development of long-lasting
193 respiratory-specific immunity.

194

195 First, we examined post-vaccination lung infiltration of antigen-experienced memory T cells.
196 These T_{RM} cells are characterized by CD69 expression as well as CD103 expression in the CD8
197 compartment (*38*). The percentage of T_{RM} cells were significantly increased in the CD8
198 compartment with i.n. vaccination (median of $CD69^+$ cells >20% of $CD8^+$) compared to i.m.
199 vaccination (median of $CD69^+$ cells <10% of $CD8^+$) following boost ($CD69^+$ $CD8^+$ cells, p =
200 0.0029; $CD69^+$ $CD103^+$ $CD8^+$ cells, $p < 0.0001$) (Figure 3A, B). While the fractions of $CD8^+$
201 T_{RM} cells were equivalent post-prime, lung expansion of T_{RM} cells followed boost administration
202 in the i.n. dosed group only, suggesting seeding of these durable populations followed by recall
203 and expansion upon boost dosing.

204

205 We then assessed $CD154^+$ $CD4^+$ T cells. CD154 (CD40 ligand [CD40L]) is often expressed on
206 activated T cells and T follicular helper cells and is critical for licensing dendritic cells and
207 engaging with B cells to enhance mucosal antibody production (*39*). Here, we found similar
208 patterns to those seen with T_{RM} cells; significantly increased populations of $CD154^+$ $CD4^+$ cells

209 were observed in the lungs after i.n. saRNA vaccination post-boost compared to i.m. vaccination

210 ($p = 0.0029$) (Figure 3C). Collectively, these data show that i.n. administration appears to elicit

211 an expansion of T_{RM} and $CD40L^+$ activated $CD4^+$ T cells within the lung. In contrast, i.m.

212 vaccination elicits minimal levels of these cell subsets, suggesting that these specialized

213 respiratory cells are not inducible by i.m. vaccination.

214

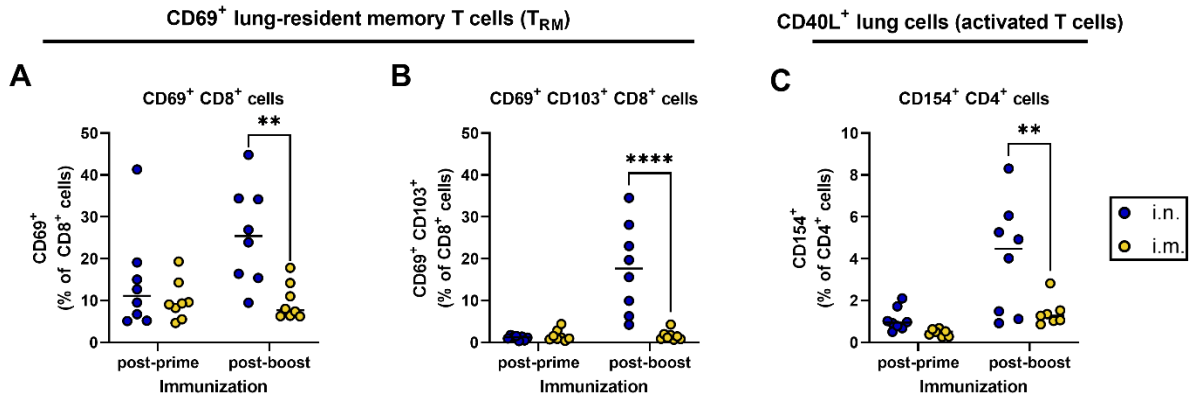

Fig. 3. Mucosal T cell populations following intranasal vaccination with SARS-CoV-2 saRNA-NLC candidate. T cell populations in the lungs were assessed 3 weeks post-prime and post-boost in C57BL/6J mice immunized with 10 µg of AAHI-SC2 either i.m. or i.n. $n = 8$ mice per group, evenly split male-female. Vector control-dosed mice were also included in the experiment and are shown in Figure 4. See Figure S3 for sample flow cytometry gating strategies. **(A-B)** $CD69^+$ lung-resident memory (A) $CD8^+$ and (B) $CD103^+$ $CD8^+$ T cells. **(C)** $CD40L^+$ ($CD154^+$)-expressing $CD4^+$ T cells. Percentage of cells in total live lung cells per mouse indicated by dots with horizontal line at median. Data were analyzed by two-way ANOVA with Sidak's multiple comparisons test. $^{**}p < 0.01$ and $^{****}p < 0.0001$.

226 *Intranasal administration elicits polyfunctional SARS-CoV-2 reactive mucosal T cell responses*

227 While the lung T cell subsets were present in large populations post-i.n. administration, we
228 wanted to verify that these cell subsets were functional effector cells and confirm that they
229 responded to SARS-CoV-2. Here, we took mice that received the vector control or had been
230 immunized and boosted with AAHI-SC2 i.m. (10 µg) or i.n. (1 µg, 5 µg, or 10 µg) and used ICS-
231 flow cytometry to determine the frequency of polyfunctional lung IFNγ$^+$IL-2$^+$TNFα$^+$ CD4$^+$ and
232 CD8$^+$ T cells following re-stimulation for 6 hours with overlapping spike peptides.
233 Polyfunctional IFNγ$^+$IL-2$^+$TNFα$^+$-secreting SARS-CoV-2 spike-responsive T cells composed a
234 large fraction of the key T_{RM}, CD69$^+$ population in the 5- and 10-µg i.n. immunized mice (12.8%
235 and 9.11%, respectively), which was significant in the CD69$^+$ CD8$^+$ subset of these T_{RM} cells
236 compared to the i.m. immunized mice (p = 0.0005 for the 5-µg dose and p = 0.0258 for the 10-
237 µg dose), as well as in the CD69$^+$ CD103$^+$ CD8$^+$ subset (p = 0.0181) from 5-µg i.n. immunized
238 mice (Figure 4A-B). Intramuscularly immunized groups again induced consistently negligible
239 levels of polyfunctional CD8$^+$ cells. We also examined the activated CD154$^+$/CD40L$^+$ CD4$^+$ T
240 cells and the lung-homing CD194$^+$/CCR4$^+$ CD4$^+$ and CD8$^+$ cells. Similar to the T_{RM} cells,
241 CD154$^+$ CD4$^+$ cells showed significantly higher percentages of polyfunctionally responding cells
242 at the 5-µg i.n. dose compared to the i.m. dose (p = 0.0006) (Figure 4C). Likewise, CD194$^+$
243 CD4$^+$ and CD8$^+$ cells were also induced by the i.n. vaccine at significantly higher percentages at
244 the 5-µg dose (p = 0.0441 and p = 0.0071, respectively) compared to the i.m. vaccine (Figure
245 4D-E).

246

247 Finally, we examined the quality of the response by lung T cells to confirm that i.n.
248 administration elicited Th1-biased lung T cell responses, like what was observed in the spleen.

249 The majority of the responses to both the i.n. and i.m. vaccines were Th1-specific responses,
250 with negligible Th2 and Th17 responses (Figure S2B), similar to what was observed in the
251 spleen. Th2 responses were not significantly different between i.m. vaccinated mice and mice
252 receiving the vaccine via the i.n. route, did not scale with increasing vaccine dose, and were not
253 significantly increased from buffer-only groups. Collectively, these data demonstrate that i.n.
254 administration seeds specialized polyfunctional $CD4^+$ and $CD8^+$ T cell populations in the lung –
255 populations which are not elicited following i.m. administration.
256

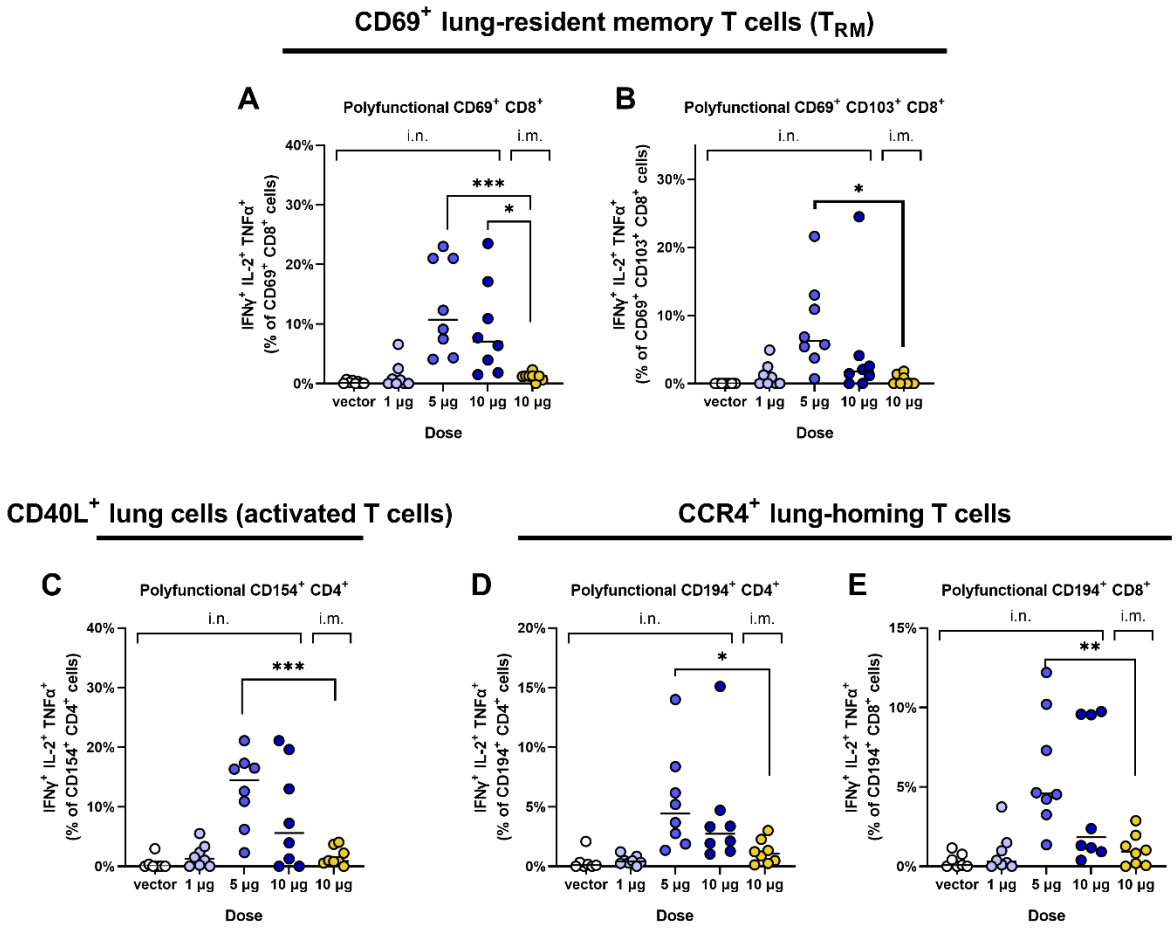

Fig. 4. Mucosal SARS-CoV-2 spike polyfunctionally reactive T cell populations following immunization with the intranasal or intramuscular SARS-CoV-2 saRNA-NLC vaccine. T cell populations in the lungs were stimulated with SARS-CoV-2 spike peptides for 6 hours and stained for T cell markers and cytokine expression 3 weeks post-boost in C57BL/6J mice immunized with 1, 5, or 10 µg of the i.n. saRNA-NLC vaccine, relative to 10 µg of the i.m. vaccine or an i.n. vector control (SEAP) saRNA-NLC. n = 8 mice for all dosing groups. Percentages of polyfunctional cells (expressing IFNγ, IL-2, and TNFα) were then measured by flow cytometry. **(A-B)** Polyfunctional CD69$^+$ lung-resident memory (A) CD8$^+$ and (B) CD103$^+$ CD8$^+$ T cells. **(C)** Polyfunctional CD40L-expressing (CD154$^+$) CD4$^+$ T cells. **(D-E)** Polyfunctional CCR4-expressing (CD194$^+$) lung-homing (D) CD4$^+$ and (E) CD8$^+$ T cells. Dots

268 represent values measured from individual mice. Horizontal lines indicate data median.

269 Significance was determined by one-way ANOVA with Tukey's multiple comparisons test: *$p <$

270 0.05, **$p < 0.01$, and *** $p < 0.001$.

271

272 *Intranasal boosting of previous i.m. vaccination induces both systemic and mucosal immune*
273 *responses*
274 To understand whether i.n. administration could be viable as a boosting strategy for individuals
275 previously vaccinated with an i.m. SARS-CoV-2 vaccine, we examined mice that were primed
276 with an i.m. vaccine and then boosted with a medium dose (5 μg) either i.m. or i.n. Intranasally
277 boosted mice showed equivalent serum anti-spike IgG levels and similar systemic neutralizing
278 antibody responses to the i.m. boosted mice (Figure 5A, B). Within the splenic $CD4^+$ and $CD8^+$
279 T cell compartment, i.n. boost immunization induced equivalent or increased spleen-resident
280 polyfunctional T cell responses in $CD4^+$ or $CD8^+$ ($p = 0.0454$) cells, respectively, compared to an
281 i.m. boost immunization (Figure 5C, D), indicating that an i.n. booster may effectively boost the
282 systemic immunity developed in response to an original i.m. vaccination. With respect to
283 mucosal immunity, the i.n. booster induced a higher but not significant percentage of $CD40L^+$
284 ($CD154^+$) activated $CD4^+$ T cells within the lungs than the i.m. booster (Figure 5E). Most
285 importantly, the i.n. booster elicited significantly more polyfunctional lung-resident $CD8^+$ $CD69^+$
286 T_{RM} cells ($p = 0.0236$) than the i.m. booster (Figure 5F), indicating that just boosting with an i.n.
287 dose may be sufficient to elicit the full mucosal immune-stimulating effect of i.n. vaccination.
288 These data are consistent with other i.n. vaccines that suggest i.n. boosting can have enhanced
289 efficacy systemically as compared to i.m. vaccines (*21*). This suggests that an i.n. boost
290 vaccination strategy may be ideal to boost systemic and induce respiratory immunity in
291 previously vaccinated individuals, reflecting the real-world scenario of second-generation SARS-
292 CoV-2 vaccine rollouts.
293

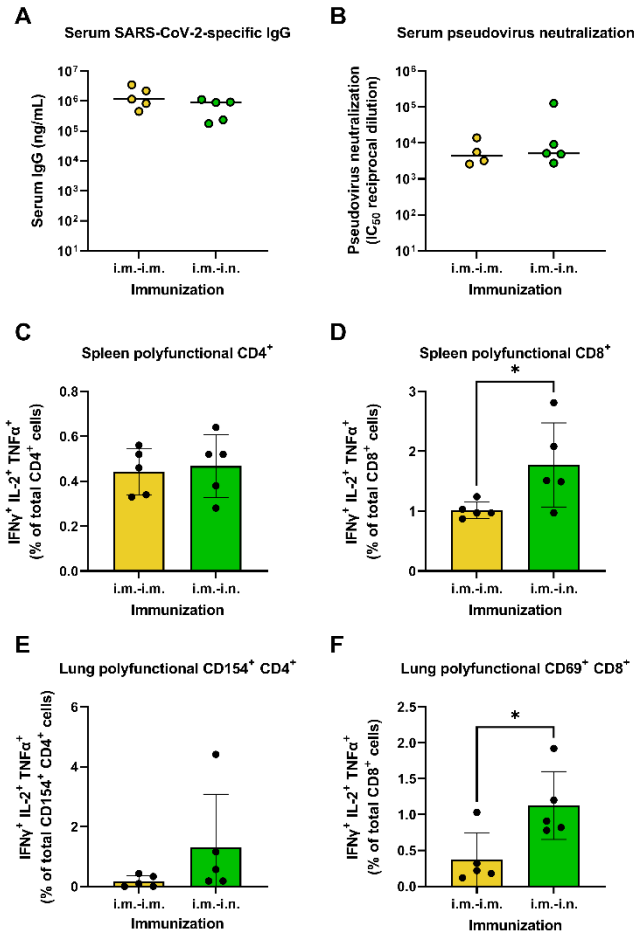

Fig. 5. Systemic and mucosal immune responses following boost immunization with the intranasal or intramuscular SARS-CoV-2 saRNA-NLC vaccines. 10-week-old C57BL/6J mice were injected i.m. with a 10-µg prime dose (N:P of 15) and then boosted with a 5-µg dose of either the i.n. or i.m. saRNA-NLC vaccine 7 weeks later. *n* = female 5 mice per group. **(A)** SARS-CoV-2 spike-specific IgG titers as measured by ELISA 3 weeks post-boost. Horizontal lines show median. **(B)** Serum SARS-CoV-2 pseudovirus neutralizing titers 3 weeks post-boost. Horizontal lines show median. **(C-D)** Spleen polyfunctional (D) $CD4^+$ and (E) $CD8^+$ T cell responses. **(E)** Polyfunctional CD40L-expressing ($CD154^+$) $CD4^+$ T cells. **(F)** Polyfunctional lung-resident memory $CD69^+$ $CD8^+$ T cell responses. Statistics evaluated as unpaired two-sided homoscedastic *t* tests, $*p < 0.05$. Bars on graphs show mean with SD.

305

306 *saRNA vaccination protects against SARS-CoV-2-induced disease in hamsters*

307 Given our data showing that i.m. prime and i.n. boost with our saRNA-NLC SARS-CoV-2
308 vaccine elicited strong systemic and pulmonary immunity in mice, we hypothesized that
309 vaccination, particularly via the i.m./i.n. route, would be sufficient to protect animals from
310 morbidity due to SARS-CoV-2 infection and would prevent these animals from transmitting the
311 virus to naive bystander animals. To test this hypothesis, we co-housed hamster pairs (1:1) for
312 several weeks to acclimate them to one another. Then, paired animals were separated and one
313 animal in each pair was either sham-vaccinated or vaccinated with 5 μg of the saRNA-NLC
314 SARS-CoV-2 vaccine given either i.m. or i.n (Figure 6A). After 24 hours, the sham-vaccinated
315 and vaccinated animals were re-paired with their naive (non-vaccinated) cagemates. On day 21,
316 peripheral blood was collected from all animals. On day 28, all pairs of animals were separated,
317 and the sham-vaccinated and vaccinated animals were boosted via the i.m. or i.n. route. All
318 animals were re-paired with their naive cagemates after 24 hours and blood was collected from
319 all animals five days later. As expected, vaccinated hamsters, particularly i.m.-dosed hamsters,
320 demonstrated strong induction of spike-specific serum IgG post-prime, which was absent in the
321 sham-vaccinated group (Figure 6B) and in all the naive cagemates (Figure S4). Intranasally
322 primed animals also showed development of significant serum IgG titers, albeit at titers
323 significantly lower than those observed in i.m.-primed animals ($p < 0.0001$). Boosting on day 28
324 did not result in a significant increase in systemic anti-spike IgG responses in any of the
325 vaccinated groups (Figure 6C), perhaps due to the still ongoing robust primary response.

326

327 At 9 days post-boost (day 37), the vaccinated and sham-vaccinated hamsters were separated from
328 their naive cagemates (Figure 6A). Some sham-vaccinated hamsters were set aside to serve as
329 uninfected negative controls (sham-vaccinated-uninfected), and all other vaccinated or sham-
330 vaccinated hamsters were experimentally infected with 1 x 10^6 pfu SARS-CoV-2 USA/WA-1
331 strain delivered intranasally. We then compared morbidity of the vaccinated-infected and sham-
332 vaccinated-infected animals to the sham-vaccinated-uninfected controls. As expected, the sham-
333 vaccinated-uninfected hamsters exhibited a modest increase in weight over the next 14 days
334 (Figure 6D). In contrast, the sham-vaccinated-infected animals had increased morbidity with
335 peak body weight loss of 9-10% by day 6 post-infection and minimal body weight recovery by
336 termination of study. The vaccinated-infected animals (i.n.-i.n., i.m.-i.n., and i.m.-i.m.
337 vaccination), on the other hand, showed minimal weight loss and exhibited rapid recovery in
338 weight by day 3-4 post-infection, with statistically significantly reduced virus infection-induced
339 morbidity when compared to the sham-vaccinated-infected group ($p = 0.0091$, $p = 0.0074$, and p
340 $= 0.0206$ for i.n.-i.n., i.m.-i.n., and i.m.-i.m. vaccinated-infected animals, respectively). Body
341 weight loss after challenge did not correlate with systemic anti-spike IgG titers, suggesting that
342 either all three vaccination regimens induced sufficient systemic IgG to protect against SARS-
343 CoV-2-induced weight loss and/or cellular or mucosal responses played a role in protection
344 (Figure S5).
345
346 To further understand the dynamics of infection and transmission, total and subgenomic viral
347 nucleocapsid (N) RNA was measured in nasal swipes from all infected hamsters across the first
348 10 days after infection. Total viral N RNA was detected in all infected hamsters as early as 1
349 hour post infection (Figure 6E), which confirmed successful intranasal instillation of SARS-

350 CoV-2. Total viral copies peaked between 24-48 hours in all infected groups. However, total
351 viral N RNA copies were significantly lower in the vaccinated-infected groups compared to the
352 sham-vaccinated-infected group ($p < 0.0001$, $p < 0.0001$, and $p = 0.0003$ for i.n.-i.n., i.m.-i.n.,
353 and i.m.-i.m., respectively). Next, subgenomic viral N RNA was quantified in the nasal discharge
354 to compare infectious, actively replicating viral load between the sham-vaccinated-infected and
355 vaccinated-infected hamsters. Subgenomic viral N RNA was detected in the nasal swipes from
356 all infected hamsters. However, significantly diminished subgenomic viral N RNA copies were
357 observed in all vaccinated-infected animals relative to the sham-vaccinated-infected animals
358 (Figure 6F) ($p < 0.0001$, $p = 0.0002$, and $p < 0.0001$ for i.n.-i.n., i.m.-i.n., and i.m.-i.m. vaccine
359 regimens, respectively). Moreover, the peak copies of subgenomic N RNA in nasal swipes were
360 observed within 24 hours of infection in the vaccinated-infected hamsters, while subgenomic N
361 RNA peaked in the sham-vaccinated-infected hamsters between days 1-2 (Figure 6F).
362 Importantly, the vaccinated-infected hamsters had increased clearance of viral subgenomic N
363 RNA that declined to undetectable levels by day 6 (i.m.-i.n. and i.m.-i.m. groups) and day 8 (i.n.-
364 i.n. group) post-infection. In contrast, the sham-vaccinated-infected control animals had
365 detectable viral subgenomic N RNA until day 10, indicating that vaccination promoted more
366 rapid reduction in replicating virus.
367
368 The viral RNA measurements from nasal swipes suggested that none of the saRNA-NLC
369 vaccination regimens induced sterilizing immunity following direct intranasal instillation with
370 $1x10^6$ pfu of SARS-CoV-2. To address whether the vaccinated animals made an immune
371 response to experimental infection, we measured systemic anti-N IgG antibodies on day 35 post-
372 infection. Indeed, anti-N IgG antibody was detected in the serum from all three groups of

373 vaccinated-infected animals (Figure 6G), indicating that the amount of N protein made by the
374 infectious virus was sufficient to elicit a *de novo* N-specific antibody response in these hamsters.
375 However, compared to the sham-vaccinated-infected animals, the amount of anti-N IgG antibody
376 was significantly lower in the i.m.-i.m. and i.m.-i.n. vaccinated-infected hamsters ($p < 0.0001$
377 and $p = 0.0470$, respectively) and modestly lower in the i.n.-i.n. vaccinated-infected hamsters,
378 again consistent with a decreased viral load in all vaccinated animals.
379
380 Next, to assess SARS-CoV-2-induced pulmonary pathology, cross sections of the hamster lungs
381 were examined and scored for histology by a board-certified pathologist. As expected, the sham-
382 vaccinated-infected hamsters had mild to moderate histology scores confirming that the SARS-
383 CoV-2 viral inoculum used to infect the hamsters caused detectable pulmonary
384 immunopathology as late as day 35 post-infection (Figure 6H). These sham-vaccinated-infected
385 hamsters exhibited signs of inflammation that consisted primarily of accumulation of
386 mononuclear and polymorphonuclear infiltrates in the alveolar interstitium and lumen, and
387 adjacent inflammation around blood vessels and bronchioles (Figure S6A). Conversely, all three
388 groups of vaccinated-infected hamsters had significantly decreased total histology scores (Figure
389 6H) and exhibited only sporadic interstitial, perivascular, and peribronchiolar inflammation
390 (Figure S6B) that were comparable to sham-vaccinated-uninfected negative control animals
391 (Figure S6C), suggesting that vaccination reduced the extent and severity of lung pathology
392 following infection with a high dose of SARS-CoV-2. Therefore, while vaccination did not
393 prevent infection following a robust viral challenge, all vaccine regimens effectively prevented
394 disease-associated morbidity as measured by weight loss, decreased peak viral copies in the nasal

395 discharge, suppression of viral replication, increased viral clearance, and protection against

396 SARS-CoV-2-induced lung damage.

397

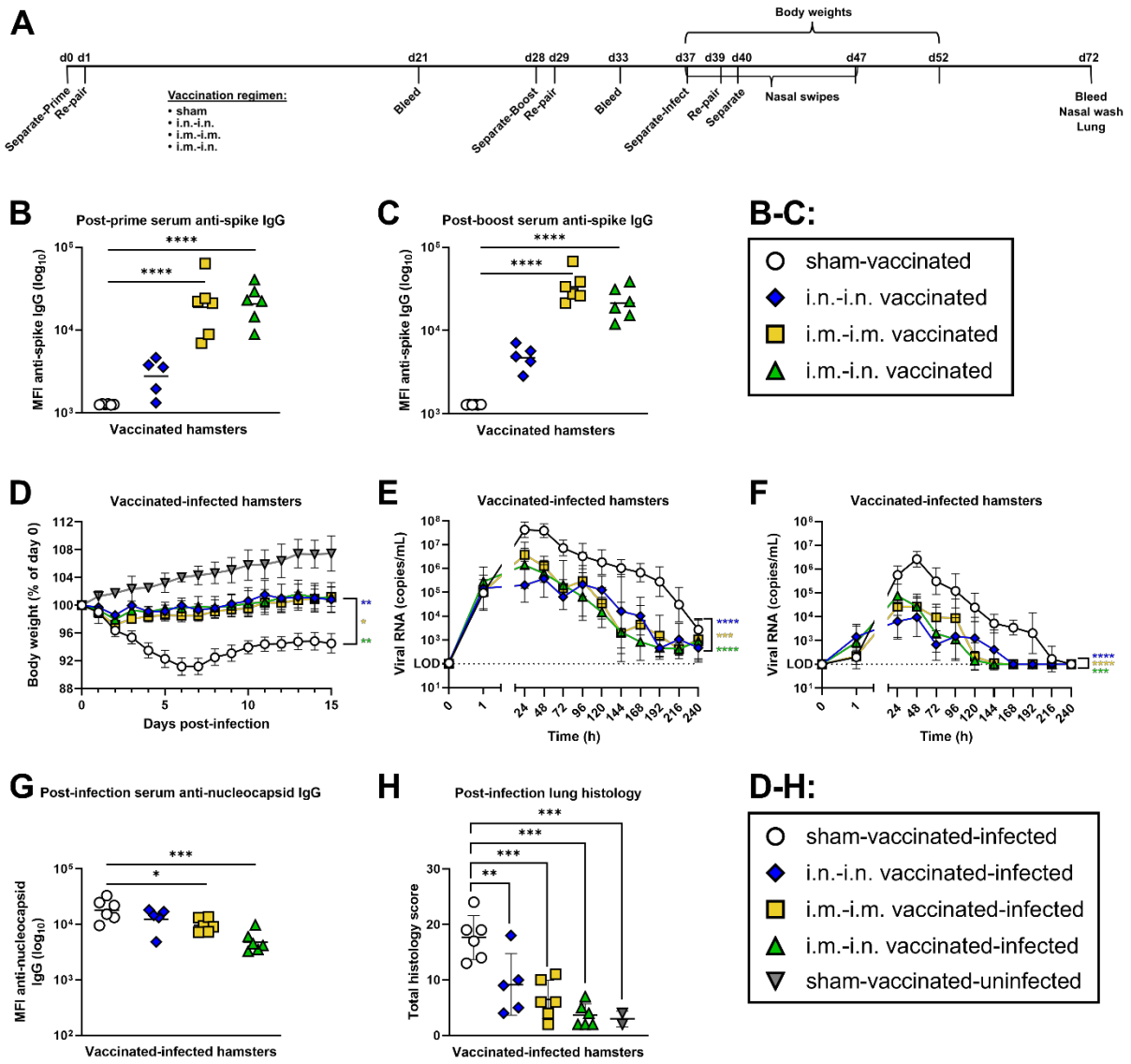

Fig. 6. Protection from SARS-CoV-2 infection-induced morbidity, viral load, and lung damage in vaccinated hamsters. (A) Study design for experiment in vaccinated and sham-vaccinated co-housed hamsters. Acclimated co-housed hamster pairs were separated on day 0. One animal in each pair was vaccinated i.n. or i.m. or was sham-vaccinated. The other animal in each pair was left untouched (naive, see Figure 7). Sham-vaccinated and vaccinated animals were re-paired with their naive cagemates on day 1. Blood was collected from all animals on day 21. Animals were separated again on day 28, and sham-vaccinated and vaccinated animals were

406 boosted either i.n. or i.m. Animals were re-paired with their naive cagemates on day 29, and
407 blood was collected on day 33. (**B-C**) Vaccine antibody responses in sham-vaccinated (open
408 black circles), i.n.-prime/i.n.-boost vaccinated (blue diamonds), i.m.-prime/i.m.-boost vaccinated
409 (yellow squares), or i.m.-prime/i.n.-boost vaccinated (green triangles) animals. n = 5-6/group.
410 Mean fluorescence intensity (MFI) of serum anti-spike IgG on day 21 **(B)** and day 33 **(C)**. Data
411 were log-transformed and assessed by two-way ANOVA with Tukey's multiple comparison test.
412 Horizontal lines show geometric mean. **(D-H)** Experimental infection in sham-vaccinated and
413 vaccinated hamsters. Vaccinated and sham-vaccinated hamsters were separated from their naive
414 cagemates on day 37 (see panel A). Two sham-vaccinated hamsters were left uninfected (grey
415 triangles, sham-vaccinated-uninfected), and all remaining sham-vaccinated and vaccinated
416 animals were experimentally infected with SARS-CoV-2 via the intranasal route. **(D)** Body
417 weight of vaccinated-infected, sham-vaccinated-infected, and sham-vaccinated-uninfected
418 hamsters. Body weight line plots show group weight mean and SEM. Body weight data was
419 analyzed on area under the curve measures, assessed statistically by one-way ANOVA with
420 Tukey's multiple comparison test. **(E-F)** Total N RNA **(E)** and subgenomic N RNA **(F)** copy
421 number in nasal swipes from vaccinated-infected and sham-vaccinated-infected hamsters. Viral
422 RNA measures were log-transformed and shown as mean and SEM. Area under the curve
423 measures were assessed with one-way ANOVA with Tukey's multiple comparison test. **(G)**
424 Anti-N IgG in serum of vaccinated-infected and sham-vaccinated-infected animals is shown as
425 MFI after log-transformation. Data statistically analyzed using one-way ANOVA with Dunnett's
426 multiple comparisons test. **(H)** Lung pathology scores were calculated for sham-vaccinated-
427 infected and vaccinated-infected animals. Horizontal lines and error bars represent mean and SD,

428 respectively. See Figure S6 for representative histopathology images. * $p < 0.05$, ** $p < 0.01$,

429 *** $p < 0.001$, **** $p < 0.0001$.

430

431 *saRNA vaccination prevents viral transmission by virally challenged hamsters*

432 Although all three groups of vaccinated-infected hamsters appeared to have been productively
433 infected following experimental SARS-CoV-2 exposure, the amount of subgenomic viral N
434 RNA in the nasal secretions of these hamsters had already declined significantly by day 2 post-
435 infection relative to the sham-vaccinated-infected group (Figure 6F). To assess whether this
436 reduction in infectious viral load was sufficient to prevent transmission, we re-paired the sham-
437 vaccinated-infected and vaccinated-infected hamsters with their naive cagemates on day 2 post-
438 infection (day 39 on timeline in Figure 6A; day 0 on timeline in Figure 7A) for a period of 24
439 hours (Figure 7A) and assessed morbidity, nasal swipe viral RNA, serum IgG antibodies, and
440 lung immunopathology in the naturally virally challenged cagemates. As expected, naive
441 cagemates of the sham-vaccinated-infected animals began losing weight within 24 hours of re-
442 pairing, reaching maximum weight loss of 6-7% by day 7 post-re-pairing and exhibiting minimal
443 body weight recovery by termination of study (Figure 7B). In striking contrast, the naive
444 cagemates of the vaccinated-infected hamsters exhibited no body weight loss following re-
445 pairing ($p = 0.0412$, $p = 0.0470$, and $p = 0.0478$ for i.n.-i.n., i.m.-i.n., and i.m.-i.m., respectively).
446

447 Given the little morbidity observed in the naive cagemates co-housed with the vaccinated-
448 infected hamsters, we hypothesized that viral transmission between the vaccinated-infected
449 animals and their naive cagemates would also be diminished. To test this, we measured total
450 (Figure 7C) and subgenomic (Figure 7D) viral N RNA in the nasal swipes from the naive
451 cagemates that were paired for 24 hours with the sham-vaccinated-infected and vaccinated-
452 infected groups. Total viral N RNA, which reflects both replicating and non-replicating virus,
453 was present in nasal swipes from all the naive cagemates as early as 24 hours post-re-pairing

454 with infected hamsters (Figure 7C). Interestingly, the naive cagemates paired with vaccinated-
455 infected hamsters had on average 70-fold lower total viral N RNA at 24 hours post-re-pairing
456 compared to naive hamsters that were co-housed with sham-vaccinated-infected animals (Figure
457 7C). Hence, immediately following re-pairing, the viral load transmitted to naive cagemates by
458 the vaccinated-infected animals was lower than that transmitted by the sham-vaccinated-infected
459 animals. Importantly, total viral N RNA in nasal secretions from the naive cagemates paired with
460 vaccinated-infected hamsters never surpassed 10^4 copies/mL (Figure 7C) and remained just
461 above the limit of detection starting at day 4 post-re-pairing ($p < 0.0001$ for all groups).
462 Conversely, the naive cagemates paired with sham-vaccinated-infected hamsters had total viral N
463 RNA nasal discharge titers that peaked at 10^7 copies/mL by day 2 post-re-pairing, with minimal
464 clearance by end of study at day 8 post-re-pairing (Figure 7C). Similarly, subgenomic viral N
465 RNA in the nasal discharge, which is indicative of viral replication/infection, was detected at 24
466 hours post-re-pairing in the naive cagemates co-housed with sham-vaccinated-infected hamsters,
467 peaked at 10^5 copies/mL by day 2-3 post-re-pairing and remained detectable even out to day 8
468 post-re-pairing (Figure 7D). This was in striking contrast to the naive cagemates of the
469 vaccinated-infected animals, which had minimal to non-detectable levels of subgenomic viral N
470 RNA in the nasal discharge (Figure 7D) ($p < 0.0001$ for all three groups).
471
472 To assess whether the naive cagemates exposed to the vaccinated-infected animals were
473 protected from active infection, we measured *de novo* anti-N serum IgG responses. As expected,
474 the naive cagemates co-housed with sham-vaccinated-infected hamsters developed high serum
475 N-specific IgG responses (Figure 7E). The naive cagemates co-housed with vaccinated-infected
476 hamsters, on the other hand, exhibited negligible responses ($p < 0.0001$ for all vaccine regimen

477 groups). Indeed, no anti-N IgG response was detected in the naive cagemates of the i.n.-i.n.
478 vaccinated-infected group, and only one naive cagemate from the i.m.-i.n and the i.m.-i.m.
479 vaccinated-infected groups developed a measurable anti-N IgG serum antibody response. Thus,
480 all three vaccine regimens were effective at preventing significant transmission of infectious
481 virus capable of inducing an immune response to naive cagemates.
482
483 Next, we compared the total histology score of each group of naive cagemates (Figure 7F).
484 Naive hamsters co-housed with the sham-vaccinated-infected hamsters exhibited mild to
485 moderate histology scores, primarily due to mild inflammation in the alveolar interstitium and
486 lumen that was similar in severity to that observed in the sham-vaccinated-infected hamsters
487 (Figure S6A). Naive hamsters co-housed with the vaccinated-infected hamsters, regardless of
488 vaccination regimen, exhibited a significantly decreased histology score ($p < 0.0001$ for all
489 vaccine regimen groups), with minimal lung pathology that was very similar to that observed in
490 the vaccinated-infected cagemates (Figure S6B). Taken together, the data demonstrate that i.m.-
491 i.m., i.n.-i.n., or i.m.-i.n. dosing of the saRNA-NLC spike vaccine was not only effective in
492 preventing disease-associated morbidity in hamsters but also prevented the vaccinated and
493 subsequently experimentally infected hamsters from transmitting infectious virus to naive
494 cagemates, even at a time when viral load peaked in the nasal discharge.
495

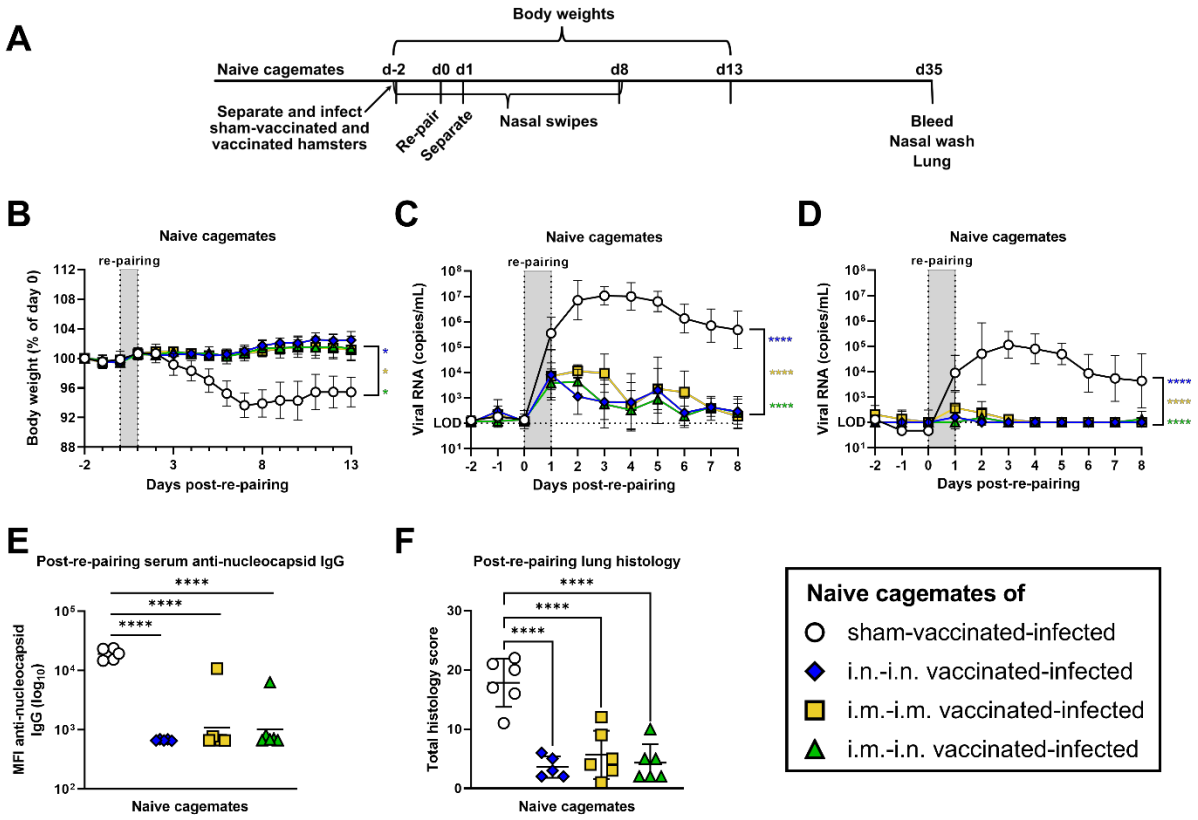

Fig. 7. Vaccination prevents transmission of SARS-CoV-2 to naive hamster cagemates. (A) Study design for transmission experiment in naive cagemates. Vaccinated and sham-vaccinated hamsters were separated from their naive cagemates on day -2 (day 37 in Figure 6A) and then experimentally infected with SARS-CoV-2. On day 0 (day 39 in Figure 6A), the naive animals were re-paired with their vaccinated-infected or sham-vaccinated-infected cagemates. On day 1 (day 40 in Figure 6A), the animals were separated and the naive cagemates were monitored for SARS-CoV-2 infection and infection-induced morbidity. **(B)** Body weight of the naive cagemates that were re-paired for 24 hours with vaccinated-infected or sham-vaccinated-infected hamsters. Body weight line plots show group weight mean and SEM. Body weight data was analyzed on area under the curve measures, assessed statistically by one-way ANOVA with Tukey's multiple comparison test. **(C-D)** Total N RNA **(C)** and subgenomic N RNA **(D)** copy

508 number in nasal swipes from naive cagemates that were re-paired for 24 hours with vaccinated-
509 infected and sham-vaccinated-infected hamsters. Viral RNA copy numbers were log-
510 transformed, and area under the curve measures are shown as mean and SEM. Data were
511 assessed with one-way ANOVA with Tukey's multiple comparison test. **(E)** Anti-N IgG in
512 serum of naive cagemates that were re-paired for 24 hours with vaccinated-infected and sham-
513 vaccinated-infected groups. Antibody levels are reported as mean fluorescence intensity (MFI)
514 following log-transformation. Data statistically analyzed using one-way ANOVA with Dunnett's
515 multiple comparisons test. **(F)** Lung pathology scores were calculated for naive cagemates that
516 were re-paired for 24 hours with sham-vaccinated-infected and vaccinated-infected animals.
517 Horizontal lines and error bars represent mean and SD, respectively. See Figure S6 for
518 representative histopathology images. * $p < 0.05$, **** $p < 0.0001$.
519

520 **DISCUSSION**

521 Here we extend previous work on this saRNA-NLC vaccine platform to show delivery of an
522 intranasal RNA vaccine that induces key respiratory mucosal immune responses. This i.n.
523 administered saRNA vaccine induced systemic immunity in both the humoral and cellular
524 compartments that rivaled i.m. administration. Additionally, i.n. administration elicited not only
525 robust populations of spike-responsive polyfunctional T cells in the spleen but also in the lung,
526 demonstrating induction of key respiratory mucosal T cell populations by an RNA vaccine (*41–*
527 *43*). Furthermore, we were able to demonstrate potential for this product as an i.n. booster of
528 prior i.m. vaccine-induced immunity, a common real-life scenario given the largely COVID-
529 experienced population at this point in the pandemic. This i.n. boost of prior i.m. vaccine-
530 induced immunity significantly boosted systemic responses in addition to inducing mucosal T
531 cell populations not stimulated by i.m. vaccine boosting. Lastly, we demonstrated that both i.n.-
532 i.n., i.m.-i.m., and heterologous i.m.-i.n. vaccination regimens prevented virus-associated
533 morbidity in the hamster model and, most importantly, prevented viral transmission and
534 development of disease in naive cagemates.

535

536 Now in the third year of the COVID-19 pandemic, second-generation SARS-CoV-2 vaccines are
537 urgently needed. While several vaccines have been developed and approved in the last 2.5 years,
538 many utilizing novel mRNA vaccine technologies (*44–46*), which have admirably contributed to
539 the waning of disease mortality globally (*47*), emerging trends highlight the insufficiencies of
540 current vaccine approaches. Vaccine efficacy has waned rapidly (*48–51*), and frequent boosters
541 have been recommended for individuals that received the Pfizer and/or Moderna mRNA
542 vaccines (*49*, *50*, *52*). Increasing evidence of reinfection, both post-infection and post-

543 vaccination (*53*), particularly with the Omicron variant (*54*), as well as ongoing viral
544 transmission post-vaccination (*55–57*), has negatively impacted vaccine credibility. With the
545 ongoing pandemic predicted to remain a present threat, new variants will continually place
546 pressure on the efficacy of these first-generation vaccines (*58*, *59*).
547
548 While more research is necessary as to why current vaccines are waning, emerging research is
549 pointing to insufficient nasal and mucosal immunity (*56*, *60*). Increasingly, data are
550 demonstrating that i.m. vaccination alone may not generate potent mucosal immunity that is
551 predicted to be critical for early control and clearance of SARS-CoV-2 (*61*). Vaccinees still show
552 evidence of viral RNA in the upper respiratory tract after viral exposure, suggesting ongoing
553 viral replication and transmission (*20*, *22*, *56*, *62*) even by vaccinated populations. However,
554 breakthrough infection with SARS-CoV-2 allows vaccinees to elicit potent mucosal and nasal
555 immunity (*41–43*). Thus, improving the induction of nasal and mucosal immunity following
556 vaccination is a critical component for second-generation vaccines to finally achieve durable and
557 flexible protection. However, data also show that generating this immunity is generally not
558 possible via standard i.m. vaccination and likely requires administration of an i.n. vaccine (*60*,
559 *63*).
560
561 Intranasal vaccines to date have primarily been developed as live-attenuated flu vaccines,
562 including FluMist (*64*). Recently, four new i.n. or inhalable vaccines have been approved for
563 SARS-CoV-2 in China, India, Iran, and Russia, including two adenovirus-vectored vaccines (*65–*
564 *67*). Further development of nasal or airway administration of vaccines for influenza and other
565 respiratory viruses has remained an attractive target given the potential for development of

566 critical airway T_{RM} cells at this first line of defense (*3*, *68*). Several other i.n. vaccines are in
567 development for SARS-CoV-2, but most rely on standard protein or adenovirus vector vaccine
568 technologies (*20*, *21*, *43*, *69*, *70*). An RNA-based vaccine, in contrast, can be developed more
569 rapidly, and allows cross-over i.m. to i.n. vaccination without developing a new vaccine,
570 allowing for significantly greater utility in pandemic situations. The thermostability and
571 stockpiling ability of our saRNA-NLC vaccine platform additionally provide key attributes for
572 rapid and widespread pandemic response (*11*, *17*). Validating an RNA-based, i.n. administered
573 vaccine technology would be a significant development not only for the SARS-CoV-2 pandemic
574 but for other respiratory pathogens, combining the rapidity and reliability of RNA vaccine
575 adaptation to new targets with the key mucosal immune responses induced by mucosal-specific
576 dosing.
577
578 AAHI's SARS-CoV-2 saRNA-NLC vaccine candidate elicits both robust systemic humoral
579 immunity and spike-responsive systemic polyfunctional T cells as an i.m. or i.n. vaccine.
580 Delivered i.n., it also elicits tissue-resident T cell populations within the lungs, suggesting broad
581 T cell presence across the respiratory tract – an effect that i.m. delivered mRNA vaccines have
582 been unable to induce to date (*41–43*). While CD4 and CD8 T cell populations are now being
583 recognized as a major determinant of disease progression and critical to long-lasting immunity
584 (*13*), the main vaccines on the market elicit minimal peripheral T cell responses (*71*, *72*) and
585 negligible mucosal/respiratory T cell responses (*41–43*). The thermostability and ability to
586 administer i.n. may make this vaccine substantially more desirable in the fight against respiratory
587 viruses. These data demonstrate the potential for this i.n. saRNA-NLC vaccine candidate as an
588 effective booster to pre-existing SARS-CoV-2 immunity, outperforming an i.m. booster,

589 showing that the additive effect of this i.n. vaccine to pre-existing systemic immune responses
590 generated the greatest benefit of all vaccination regimens tested.
591
592 These data demonstrate that all immunization methods elicited full protection against virus-
593 associated morbidity and viral transmission. While our original hypothesis was that only i.n.
594 vaccination would prevent transmission, we were pleasantly surprised that all three delivery
595 methods prevented transmission. These data bolster the overall strength of the vaccine by
596 demonstrating that i.m. vaccination is protective as well. While it is unclear the specific cellular
597 or serum components mediating this protection in i.m. vaccinated animals, which lack substantial
598 lung T_{RM} cell populations and significant mucosal IgA, it may be that sufficiently high systemic
599 IgG so early after boost (9 days post-boost) may circulate and prevent transmission (*73*, *74*).
600 Future studies examining protection and transmission by vaccinated hamsters at longer
601 timepoints post-vaccination may more fully demonstrate the advantages of i.n. vaccine
602 administration and induction of mucosal immunity on protection and transmission prevention
603 relative to i.m.-i.m. or heterologous i.m.-prime, i.n.-boost vaccine regimens.
604
605 The i.n. saRNA vaccine may be most effective as a booster dose following an i.m. prime. This
606 aligns with the results of other studies (*14*, *62*, *75*) where priming an immune response with a
607 strong i.m. vaccine followed by i.n. vaccination is able to optimally stimulate the T_{RM}
608 compartment while still boosting the extant i.m. induced immunity. Our data demonstrate the
609 clear potential of using an identical or similar RNA vaccine product for both i.m. and i.n.
610 vaccination, potentially eliminating many manufacturing hurdles and using an already clinically
611 tested vaccine platform technology (*76*) for multiple routes of administration. In our studies, i.n.

612 boosting outperformed i.m. boosting particularly in mucosal immune measures, hinting at the
613 potential for i.n. dosing to access novel cell compartments and mechanisms. Further work
614 remains to fully optimize the i.n. saRNA vaccine formulation specifically for i.n. administration,
615 potentially including use of nasal spray devices, with the goal of enhancing induction of
616 immunity while avoiding toxicity and reducing heterogeneity in nasal delivery. As a first step in
617 this further development process, this i.n. SARS-CoV-2 vaccine candidate is being tested in
618 nonhuman primate studies to enable future human testing.
619
620 While these studies have been carefully designed and carried out to maximize scientific rigor and
621 reproducibility, they do have certain limitations. While we showed robust systemic and mucosal
622 immunity, protection, and transmission prevention, these data are developed in mice and
623 hamsters, and these responses may not translate fully to primates and humans. Ongoing studies
624 have been designed to investigate this issue. Our data are also limited by the heterogeneity in
625 mouse immune responses when vaccinated i.n., related to a lack of consistent dosing devices for
626 i.n. vaccination. Similarly, because mice are obligate nasal breathers (*77*) and vaccine volumes
627 are difficult to appropriately scale to mouse size, some potential exists for delivery of a fraction
628 of the vaccine volume beyond the nasal tract to the lungs and digestive tract. These issues are
629 likely only resolvable with larger animal models better representing the nasal passages and
630 respiratory tracts of humans, and use of appropriate delivery devices for improvement in vaccine
631 dose delivery. Similarly, some toxicity was noted in the highest i.n. delivered saRNA-NLC
632 vaccine dose (10 μg) in mice, resulting in notable transient mouse weight loss. While these
633 effects are not expected to scale to primates due to non-linear dose scaling of saRNA vaccines
634 relative to animal size and nasal tissue surface area, any potential toxicity noted with an i.n.

635 vaccine will be closely monitored in future studies, and further optimization of the NLC
636 formulation specifically for i.n. delivery will also be conducted to minimize any such effects.
637 Finally, we have been unable to test this saRNA-NLC vaccine candidate head-to-head against
638 any commercially available SARS-CoV-2 vaccines for comparison of either vaccine
639 immunogenicity or efficacy due to restrictions on vaccine sale and research use. Should such
640 comparisons become more feasible in the future, we anticipate them to greatly benefit future
641 work, including enabling further exploration of the use of this i.n. saRNA vaccine as an effective
642 mucosal immunity-inducing booster of prior approved SARS-CoV-2 vaccination.
643
644 This saRNA-NLC vaccine platform represents a promising technology to combat both the
645 existing SARS-CoV-2 pandemic and other respiratory illnesses, such as seasonal and pandemic
646 influenza. For respiratory pathogens, i.n. vaccination or i.n. vaccine boosting of i.m. vaccination
647 may help raise RNA vaccine technologies to a new level, through stimulating respiratory T cell
648 and B cell populations (*27*, *78*, *79*) and generating effector subsets within the lungs and nasal
649 mucosa primed to respond rapidly at the first point of infection (*62*). Beyond its efficacy at
650 stimulating T_{RM} subsets and bolstering systemic immunity, i.n. administration may also be
651 desirable as a needle-less delivery method with potentially higher uptake, particularly in
652 pediatric and vaccine-hesitant populations. Altogether, this novel demonstration of a unique i.n.
653 delivered RNA vaccine that elicits strong systemic and mucosal immunity is an indication of a
654 promising new technology ripe for future development and application.
655

656 **MATERIALS AND METHODS**

657 *Study design*

658 Research objectives

659 This study was designed to test the immunogenicity and efficacy of i.n. and i.m. delivered
660 SARS-CoV-2 saRNA-NLC vaccines in mice and hamsters. Our hypothesis prior to the study
661 initiation was that i.n. delivery of this saRNA vaccine would elicit superior respiratory immunity
662 in rodents, specifically eliciting long-lived memory T cells, while possibly driving systemic
663 immune responses, even if not at the level induced by standard i.m. delivery of the vaccine.
664 Furthermore, we believed that the i.n. delivered vaccine would therefore elicit protection from
665 morbidity in the hamster model and superior reduction in viral transmission relative to the i.m.
666 delivered vaccine. As the data developed, we further hypothesized that heterologous dosing of
667 the vaccine, with an i.m. prime and i.n. boost, would combine the best attributes of both vaccine
668 delivery methods and elicit a combination of systemic and respiratory immune responses that
669 would optimally protect against viral challenge and transmission.

670

671 Research subjects or units of investigation

672 Research was conducted on C57BL/6J mice obtained from The Jackson Laboratory. Lakeview
673 Golden (LVG) Syrian hamsters were obtained from Charles River Laboratories.

674

675 Experimental design

676 We conducted several mouse vaccine immunogenicity experiments to address these questions,
677 vaccinating mice i.m and/or i.n. with our SARS-CoV-2 saRNA vaccine. Mice were vaccinated
678 using different doses and dosing strategies (homologous vs. heterologous prime-boost vaccine

679 regimens), and immunogenicity was assessed by ELISA and pseudoneutralization assay on
680 serum samples, T cell intracellular cytokine staining (ICS) on spleen and lung samples, bone
681 marrow B cell ELISpot, and T cell ELISpot to assess systemic antibody responses and induction
682 of specific vaccine-induced T cell and B cell populations.
683
684 Randomization
685 Rodents were obtained commercially and randomized into study groups prior to study onset.
686
687 Blinding
688 Investigators were not blinded to the study groups during data collection and analysis as this is
689 typically unnecessary for this type of inbred animal study and introduces more systemic and
690 human error than it prevents. Quantitative, unbiased assays were developed with highly regulated
691 SOPs in order to minimize data biases.
692
693 Sample size
694 Statistical analyses have been the guiding strategy to maximize statistical power while reducing
695 the number of animals used to a minimum. We have previously determined that 6-8 animals per
696 group (3-4 male, 3-4 female) is the lowest estimate to achieve meaningful comparisons between
697 vaccine candidates with subtle differences in immunogenicity. 10 mice/group, 5 male and 5
698 female, is required to provide statistical power of 90% with an alpha (p-value) of 0.05 to detect a
699 statistically significant difference in pseudovirus neutralizing antibody titers between vaccinated
700 groups with two-fold differences in mean antibody titers with expected statistical variance. We
701 use both male and female mice in most study groups to avoid sex-driven data biases and allow

702 for identification of any sex-specific differences in vaccine immunogenicity. For one select study
703 where mouse numbers were limited (Figure 5), $n = 5$ all-female mice were used per group to
704 provide statistical power of 80% to detect two-fold differences in serum antibody titers. The use
705 of all female mice in this study was conducted in order to reduce data variability sufficiently to
706 minimize animal use without compromising the main study immunogenicity readouts.
707
708 Data inclusion/exclusion criteria
709 No data were excluded from any plots or analyses except two cases: (1) for flow cytometry after
710 ICS where <50,000 cells were collected in the well (this was established as a guideline
711 prospectively) and (2) one i.n. vaccinated hamster was removed from Figure 6 where the
712 complete lack of anti-spike IgG antibody established that it had not been effectively vaccinated.
713
714 Outliers
715 Our policy prior to study initiation was not to exclude any outliers. Therefore, we have not
716 excluded any outliers. Assays were repeated on any suspected outliers in order to verify data
717 prior to inclusion.
718
719 Replicates
720 Replication of data was conducted whenever possible. All experiments were conducted with a
721 minimum of biological triplicates. ELISAs and pseudoneutralization assays were conducted with
722 technical duplicates for each study sample. T cell immunogenicity was only assessed in technical
723 singlicate due to limiting tissue quantity and cell number. Bridging groups were used between

724 independent animal studies to provide replication of key study groups across multiple studies
725 offset by months. All attempts at replication verified the robustness of the scientific approach.
726
727 *saRNA expression plasmid design, cloning, and production*
728 The saRNA plasmid was designed and selected based on immunogenicity measures from i.m.
729 immunization (*11*). Briefly, the saRNA encodes a SARS-CoV-2 spike sequence based on a
730 GenBank sequence (MT246667.1) containing the D614G mutation, a diproline at sites 987-988,
731 and a QQAQ substitution for RRAR in the furin cleavage site (683-686). The sequence was
732 codon-optimized for expression in humans, synthesized by BioXp, and inserted via Gibson
733 cloning into AAHI's backbone saRNA expression vector. A SEAP-expressing plasmid was also
734 used as a control, created similarly with the SEAP sequence in the place of the vaccine antigen.
735 Sanger sequencing was used to confirm plasmid sequences. These were then amplified in
736 *Escherichia coli* and extracted using Qiagen maxi- or gigaprep kits, linearized with NotI (New
737 England Biolabs), and purified using a Qiagen DNA purification kit.
738
739 *RNA manufacture*
740 NotI-linearized DNA plasmids containing T7 promoters were used as templates for *in vitro*
741 transcription (IVT) of saRNA for vaccination. Our in-house optimized IVT protocol with T7
742 polymerase, RNase inhibitor, and pyrophosphatase (Aldevron) was used. Next, a Dnase step was
743 used to digest the templates, and Cap0 structures were added to the RNA transcripts with
744 guanylyltransferase (Aldevron), GTP, and S-adenosylmethionine (New England Biolabs).
745 CaptoCore 700 resin (GE Healthcare) was used to chromatographically purify the RNA followed
746 by diafiltration and concentration. saRNA material was filtered through a 0.22-µm

747 polyethersulfone filter and stored at −80°C until further use. saRNA size and integrity was
748 characterized by gel electrophoresis, and RNA concentration was quantified by UV absorbance
749 (NanoDrop 1000) and RiboGreen assay (Thermo Fisher).
750
751 *NLC manufacture*
752 A mixture of trimyristin (IOI Oleochemical), squalene (Sigma-Aldrich), sorbitan monostearate
753 (Sigma-Aldrich), and the cationic lipid 1,2-dioleoyl-3-trimethylammonium-propane (DOTAP;
754 Corden) was heated at 70°C in a bath sonicator. Separately, polysorbate 80 (Fisher Scientific)
755 was diluted in 10 mM sodium citrate trihydrate and heated to 70°C in a bath sonicator. After all
756 components were in suspension, a high-speed laboratory emulsifier (Silverson Machines)
757 running at 7,000 rpm was used to blend the oil and aqueous phases. Particle size of the mixture
758 was further decreased through high-shear homogenization. The colloid mixture was then
759 processed at 30,000 psi for 11 discrete microfluidization passes using an M-110P microfluidizer
760 (Microfluidics). The NLC product was then filtered through a 0.22-µm polyethersulfone filter
761 and stored at 2°C–8°C until use (*11*, *17*, *80*).
762
763 *Vaccine complexing and characterization*
764 Vaccine complexes were produced by combining aqueous RNA at a 1:1 volume ratio with NLC
765 that was pre-diluted in a 10 mM sodium citrate and 20% w/v sucrose buffer. Vaccines were
766 prepared at a nitrogen:phosphate (N:P) ratio of 5-15, representing the ratio of amine groups on
767 the NLC DOTAP to the RNA's backbone phosphate groups. This complexing resulted in vaccine
768 containing the intended dose of complexed saRNA-NLC in an isotonic 10% w/v sucrose, 5 mM

769 sodium citrate solution. The vaccine solution was incubated on ice for 30 minutes after mixing to
770 ensure complete complexing.
771
772 *Mouse studies*
773 All mouse work was done according to the Bloodworks Northwest Research Institute's
774 Institutional Animal Care and Use Committee. All mouse work was in compliance with all
775 applicable sections of the Final Rules of the Animal Welfare Act regulations (9 CFR Parts 1, 2,
776 and 3) and the *Guide for the Care and Use of Laboratory Animals* (*81*).
777
778 C57BL/6J mice purchased from The Jackson Laboratory were used for all mouse studies. Mice
779 were between 6 and 8 weeks of age at study onset and evenly split between male and female. At
780 arrival, mice were simultaneously randomized into study groups, half male and half female,
781 housed separately 3-5 mice per cage with irradiated bedding in Allentown individually ventilated
782 cages. Sterile water gel packs were given to all newly arrived animals during the acclimation
783 period, and animals had access to fresh potable water *ad libitum* via Edstrom automatic reverse-
784 osmosis and chlorinated water system. Cages were changed every 2 weeks inside a laminar flow
785 cage change station. A spot check for dirty cages was conducted on the non-change weeks.
786
787 Mice were observed daily for 3 days post-injection after both prime and boost injections by
788 trained personnel. Isoflurane delivered by inhalation was used for temporary anesthesia
789 immediately prior to retro-orbital blood collection and i.n. immunization to mitigate animal pain
790 and distress. At study completion, animals were humanely euthanized by CO_2 overdose.
791

792 Animal handling technicians were not blinded to study groups. After 1 week of acclimatization
793 to the facility, mice were then primed with vaccine. Mice were then boosted 3 weeks later and
794 harvested 3 weeks after boost. Mouse weights were monitored for 4 days following prime and
795 boost vaccinations. Mice were immunized by i.m. injection in both rear quadriceps muscles (50
796 µL/leg, 100 µL total) or by i.n. inoculation in two 25-µL doses. Intranasal inoculation was done
797 under full anesthesia, and mice were allowed to recover under a heat lamp. During ongoing
798 studies, serum samples were taken by retro-orbital bleed. Three-weeks post-boost, mice were
799 harvested, terminal bleeds were taken, spleens and lungs were dissected, and femurs were
800 harvested for bone marrow purification.
801
802 *Mouse serum IgG, IgG1, and IgG2a titers by ELISA*
803 SARS-CoV-2 spike-specific IgG was measured by ELISA. Plates (Corning 384-well high-
804 binding #CLS3700) were coated with Recombinant SARS-Cov-2 Spike His Protein, Carrier Free
805 (R&D Systems #10549-CV), at 1 µg/mL and incubated overnight at 4°C. Plates were incubated
806 in blocking buffer (2% dry milk, 0.05% Tween 20, 1% goat serum) for over 1 hour. Samples
807 were plated on low-binding plates, starting at a dilution of 1:40 and then serially diluting 1:2
808 across the plate. High-binding plates were washed, and samples were then transferred from the
809 low-binding plates to the coated, high-binding plates. Naive mice serum at 1:40 was used as a
810 negative control. A SARS-Cov-2 neutralizing monoclonal antibody (GenScript #A02057) was
811 used as a positive control at a starting concentration of 3.2 ng/µL. Following a 1-hour incubation,
812 plates were washed, and a secondary antibody, Anti-Mouse IgG (Fc Specific)-Alkaline
813 Phosphatase antibody (Sigma-Aldrich #A2429), at a 1:4000 dilution was added. Following the
814 secondary antibody and another wash step, phosphatase substrate tablets (Sigma-Aldrich

815 #S0942) were dissolved in diethanolamine substrate buffer (Fisher Scientific #PI34064) at a final
816 concentration of 1 mg/mL and added to the plates. Plates were incubated for 30 minutes and then
817 read spectrophotometrically at 405 nm. A 4-point logistic (4PL) curve was used to fit the
818 antibody standard titration curve, and sample concentrations were interpolated off the linear
819 region of the curve.
820
821 For IgG1 and IgG2a isotype-specific ELISAs, plates were coated and blocked as described
822 above. For IgG1 and IgG2a, the standard curve was run using SARS-CoV-2 neutralizing
823 antibodies (GenScript #A02055 and #BS-M0220, respectively). Sample dilution and incubation
824 were identical to the total IgG curve, and plates were probed with IgG1- and IgG2a-specific
825 secondary alkaline phosphatase (AP)-conjugated detection antibodies (Sigma-Aldrich
826 #SAB3701172 and #SAB3701179, respectively) prior to development, reading, and
827 quantification as described above.
828
829 *Pseudovirus neutralization assay*
830 SARS-CoV-2 pseudovirus neutralizing antibody titers in mouse sera were measured via a
831 pseudoneutralization assay (*82*). Lentiviral SARS-CoV-2 spike protein pseudotyped particles
832 were prepared by co-transfecting HEK-293 cells (American Type Culture Collection CRL
833 #11268) with plasmids containing a lentiviral backbone-expressing luciferase and ZsGreen (BEI
834 Resources #NR-52516), lentiviral helper genes (BEI Resources #NR-52517, NR-52518, and NR-
835 52519), or a delta19 cytoplasmic tail-truncated SARS-CoV-2 spike protein (Wuhan strain
836 plasmids from Jesse Bloom of Fred Hutchinson Cancer Center). Cells were incubated for 72
837 hours at standard cell culture conditions (37°C, 5% CO_2), and cell culture media were harvested

838 and filtered through a 0.2-µm filter. Pseudovirus-containing supernatant was frozen until titering
839 and use.
840
841 To perform the assay, plates were seeded with Human Angiotensin-Converting Enzyme 2
842 (hACE2)-expressing HEK-293 cells (BEI Resources #NR52511) and incubated overnight.
843 Serum samples were pre-diluted 1:10 in media (Gibco Dulbecco's Modified Eagle Medium +
844 GlutaMAX + 10% fetal bovine serum [FBS]) and then serially diluted 1:2 for 11 total dilutions.
845 These were then incubated with polybrene (Sigma-Aldrich #TR-1003-G) and pseudovirus for 1
846 hour. Then, the serum samples were added onto the hACE2 cells in duplicate and incubated at
847 37°C and 5% CO_2 for 72 hours. To determine 50% inhibitory concentration (IC_{50}) values, plates
848 were scanned on a fluorescent imager (Molecular Devices ImageXpress Pico Automated Cell
849 Imaging System) for ZsGreen expression. Total integrated intensity per well was used to
850 calculate the percent of pseudovirus inhibition per well. Neutralization data for each sample were
851 fit with a 4-parameter sigmoidal curve, which was used to interpolate IC_{50} values.
852
853 *Spleen, lung, and bone marrow cell harvest*
854 Spleens were prepared in 4 mL of RPMI medium by manual maceration through a filter using
855 the back of a syringe. Dissociated splenocyte samples were centrifuged briefly at 400 x g to
856 pellet fat cells, and the supernatants containing lymphocytes were either transferred to 5-mL
857 mesh-cap tubes to strain out any remining tissue debris or lysed with ammonium-chloride-
858 potassium (ACK) lysing buffer. Cells were counted on a Guava easyCyte cytometer (Luminex)
859 and plated in round-bottom 96-well plates at 1-2 x 10^6 cells per well in complete RPMI (cRPMI)
860 medium containing CD28 costimulatory antibody (BD Biosciences #553294) and brefeldin A.

861 One of three stimulation treatments was added to each well: 0.0475% dimethyl sulphoxide
862 [DMSO], 2 µg/µL spike peptide pool (JPT peptides #PM-WCPV-S-1), or phorbol myristate
863 acetate (PMA)-ionomycin. Plates were incubated for 6 hours at 37 C with 5% CO_2.
864
865 Lung cells were isolated via enzymatic digestion using a gentleMACS Dissociator (Miltenyi
866 Biotec). Lungs were dissociated in 4 mL of Hanks' Balanced Salt Solution (HBSS)
867 supplemented with 10% Liberase (MilliporeSigma), 10% aminoguanidine, 0.1% KN-62, and
868 1.25% Dnase. Lungs and enzymatic mix were added to a gentleMACS M tube (Miltneyi Biotec),
869 and the m_lung_01.02 program was run. Samples were then incubated at 37°C and 5% CO_2 for
870 30 minutes. Directly after, samples were run again on the gentleMACS Dissociator using the
871 m_lung_02.01 program. The resulting slurry was added to 10 mL of RPMI medium and
872 centrifuged for 5 minutes. The supernatant was discarded, and the cells were either filtered
873 through a 5-mL snap-top tube or washed again in RPMI medium prior to counting on a Guava
874 easyCyte cytometer and plated in round-bottom 96-well plates at 1-2 x 10^6 cells per well in RPMI
875 medium containing 10% FBS, 50 µM beta-mercaptoethanol, CD28 costimulatory antibody,
876 brefeldin A, and one of three stimulation treatments: 0.0475% DMSO, 2 µg/µL spike peptide
877 pool (JPT peptides #PM-WCPV-S-1), or PMA-ionomycin. Plates were incubated for 6 hours at
878 37 C with 5% CO_2.
879
880 *Intracellular cytokine staining and flow cytometry*
881 Following incubation, plates were centrifuged at 400 x g for 3 minutes, the supernatants were
882 removed, and cells were resuspended in phosphate-buffered saline (PBS). Splenocytes were
883 stained for viability with Zombie Green (Biolegend) in 50 µL of PBS. Cells were washed twice,

884 and then spleen samples were incubated with CD16/CD32 antibody (Invitrogen #14-0161-86) to
885 block Fc receptors. Next, the cells were surface stained in an additional 50 μL of staining buffer
886 (PBS with 0.5% bovine serum albumin and 0.1% sodium azide). Spleen samples were stained
887 with fluorochrome-labeled monoclonal antibody (mAb) specific for mouse CD4 (eBioscience
888 #45-0042-82), CD8 (BD Biosciences #563068), CD44 (BD Biosciences #560568), and CD107a
889 (BioLegend #121614), while lung samples were stained for CD4 (BioLegend #100526), CD8
890 (BD Biosciences #563068), CD44 (BD Biosciences #562464), CD69 (BioLegend #104508),
891 CD103 (BioLegend #121435), CD194 (BioLegend #131220), and CD154 (BD Biosciences
892 #745242). Cells were washed twice, permeabilized using the Fixation/Permeabilization Kit (BD
893 Biosciences #554714), and stained intracellularly. Spleens were stained for TNFα (BioLegend
894 #506327), IL-2 (BioLegend #503824), IFNγ (Invitrogen #25731182), IL-5 (eBioscience #12-
895 7052-82), IL-10 (BD Biosciences #564081), and IL-17a (BD Biosciences #560820), while lungs
896 were stained for TNFα (BioLegend #506327), IL-2 (BioLegend #503824), IFNγ (Invitrogen
897 #25731182), IL-5 (BioLegend #504306), and IL-17a (BD Biosciences #560820). After two
898 washes in staining buffer, cells were resuspended in 100 μL of staining buffer and analyzed
899 using an LSRFortessa flow cytometer (BD Biosciences). After initial gating for live $CD4^+$ or
900 $CD8^+$ lymphocytes, cells gating positive for all three activation markers IL-2, IFNγ, and TNFα
901 were counted as activated polyfunctional T cells.
902
903 *Bone marrow harvest and ASC ELISpot*
904 Antibody-secreting bone marrow-resident cell counts were measured by ELISpot.
905 $MultiScreen_{HTS}$ IP Filter plates (0.45 μm, MilliporeSigma) were treated with 15 μL of 35%
906 ethanol for 30 seconds. Recombinant SARS-CoV-2 Spike His Protein, Carrier Free (R&D

907 Systems #10549-CV-100), was diluted at 2 µg/mL in ELISpot coating buffer (eBioscience), and
908 plates were coated with 100 µL. Plates were incubated overnight at 4°C. The next day, plates
909 were washed with PBS with 0.1% Tween 20 and blocked with cRPMI medium for 2 hours.
910
911 Femurs were removed from mice and inserted into a snipped-end 0.6-mL Eppendorf tube and
912 then inserted into a 1.5-mL Eppendorf tube with 1 mL of cRPMI medium. Femurs were
913 centrifuged for 15 seconds at 10,000 rpm, and supernatant was discarded. Cell pellets were
914 vortexed, resuspended in 200 µL of RBC Lysis Buffer (Invitrogen), and then incubated on ice for
915 30 seconds. An additional 800 µL of RPMI medium was added, and cells were centrifuged for 5
916 minutes at 400 x g before the supernatant was decanted. Cells were resuspended in 1 mL of
917 cRPMI medium, counted, and transferred to prepared filter plates at 1 million cells per well
918 followed by a 3-fold dilution across five adjacent wells.
919
920 Plates were incubated for 3 hours, then washed three times with PBS plus 0.1% Tween 20.
921 Secondary antibody (Goat Anti-Mouse IgG-HRP or IgA-HRP [SouthernBiotech #1030-05 and
922 #1040-05, respectively]) was added at a 1:1000 dilution in PBS with 0.1% Tween and 5% FBS
923 overnight at 4°C. Plates were then washed three times in PBS with 0.1% Tween 20 and two
924 times in PBS. 100 µL of Vector NovaRED Substrate Peroxidase (Vector Laboratories #SK-
925 4800) was applied for 7 minutes to develop the plates. The reaction was quenched by rinsing
926 plates with distilled water for 2 minutes, and plates were dried in the dark. Spots were counted
927 and data were analyzed using ImmunoSpot v7 software (Cellular Technology Limited).
928

929 *T cell ELISpot assay*

930 IFNγ (BD Biosciences #51-2525KZ), IL-17A (Invitrogen #88-7371-88), or IL-5 (BD
931 Biosciences #51-1805KZ) at a 1:200 dilution in Dulbecco's PBS (DPBS; Gibco) was used to
932 coat ELISpot plates (MilliporeSigma). Plates were incubated overnight at 4°C and then washed
933 and blocked with cRPMI medium for at least 2 hours. Previously harvested splenocytes (see
934 above) were added at 2 x 10^5 cells per well. Samples were then stimulated with 1 µg/mL PepMix
935 SARS-CoV-2 (JPT Peptide Technologies #PM-WCPV-S-1). Plates were incubated at 37°C and
936 5% CO_2 for 48 hours. Then plates were washed with PBS with 0.1% Tween 20. Next, detection
937 antibody (IFNγ, BD Biosciences #51-1818KA; IL-17A, Invitrogen #88-7371-88; and IL-5, BD
938 Biosciences #51-1806KZ) was diluted in ELISpot diluent (eBiosciences) at 1:250 and added
939 overnight at 4°C. Plates were washed and then developed using Vector NovaRED Substrate
940 Peroxidase for 15 minutes. The reaction was quenched with deionized water. Plates were then
941 dried in the dark. Spots were counted and data were analyzed using ImmunoSpot.

942

943 *Hamster studies*

944 Nine-week-old male Lakeview Golden (LVG) Syrian hamsters were purchased from Charles River
945 Laboratories and maintained in the University of Alabama at Birmingham (UAB) animal facilities,
946 which include the UAB Southeastern Biosafety Lab (SEBLAB) ABSL3 facilities. All hamster
947 procedures were approved by the UAB Institutional Animal Care and Use Committee (IACUC
948 protocol 22628) and the UAB Biosafety Committee (Protocol 22-160 and 22-161). All procedures
949 were performed in accordance with National Resource Council guidelines.

950

951 *Hamster vaccination and infection*

952 Adult male hamsters were housed in pairs and separated at the time of vaccination. One hamster
953 from each pair was vaccinated with 5 mg of saRNA-NLC delivered i.m. (50 mL per rear quadriceps
954 muscle, 100 mL total) or i.n. (25 mL/nare, 50 mL total). Sham-vaccinated hamsters received dPBS
955 i.m. Vaccinated and sham-vaccinated animals were re-paired with naive cagemates after 24 hours.
956 Cagemates were separated on day 28, and vaccinated animals were boosted with the same vaccine
957 given via the i.m. or i.n. route. Animals were re-paired after 24 hours. Nine days after the boost,
958 animals were separated, and the vaccinated and sham-vaccinated hamsters were infected i.n. with
959 1 x 10^6 pfu SARS-CoV-2 USA/WA-1 variant (50 mL/nare, 100 mL total). Uninfected controls
960 received 100 mL (50 mL/nare) of dPBS (vehicle). The infected animals were re-paired with the
961 uninfected, unvaccinated naive cagemates at 48 hours post-infection. Cagemates were separated
962 24 hours later and remained apart until the end of the study. Hamster weights were measured before
963 infection and daily until day 15 post-infection.

964

965 *Hamster blood collection and processing*

966 Blood samples from sedated hamsters were collected from the lateral saphenous vein on day 21
967 post-prime and 5 days post-boost vaccinations. Blood samples following euthanasia were collected
968 from terminal bleed via the posterior vena cava. Blood samples were transferred into BD
969 Microtainer blood collection tubes (BD Biosciences), and serum was separated by centrifugation
970 at 10,000 rpm at RT for 10 minutes. Serum samples collected post-infection were heated at 60°C
971 for 20 minutes to inactivate SARS-CoV-2 virus. All samples were aliquoted and frozen at -80°C
972 until analyzed by cytometric bead array (CBA).

973

974 *Hamster nasal viral load samples*

975 Nasal swipes were collected immediately prior to i.n. infection to establish baseline, at 1-hour
976 post-infection, and then daily until day 10 post-infection. Awake hamsters were transferred into
977 an open container to minimize movement, and the exterior surface of their nose was swiped for 5-
978 10 seconds with a polyester-tipped swab (Medical Packaging #SP-7D) that had been dipped in a
979 screw-cap tube containing 300 mL of viral transport medium (VTM; HBSS (+Ca^{2+} +Mg^{2+})
980 containing 2% FBS, 100 mg/mL gentamicin, and 0.5 mg/mL amphotericin B). The tip of the swab
981 was cut and placed inside the VTM-containing tube. The tubes were vortexed, and swab tips were
982 discarded. Samples were then processed for viral RNA quantitation.

983

984 *Hamster nasal wash samples*

985 Hamsters were sedated with isoflurane and euthanized with an intraperitoneal injection of
986 tribromoethanol (500 mg/kg, 3 mL/animal). The trachea was exposed, an incision was made, and
987 a blunt 19-gauge needle attached to a 1-mL insulin syringe was inserted into the trachea. While
988 holding the mouth of the hamster shut with one hand, 400 mL of VTM was squeezed through the
989 nasal passages, out of the nose, and into a screw-cap tube. Samples were heated at 60°C for 20
990 minutes to inactivate SARS-CoV-2 virus, then aliquoted, and stored at -80°C until analyzed by
991 CBA.

992

993 *Recombinant SARS-CoV-2 spike, RBD, and N protein production*

994 Recombinant SARS-CoV-2 spike ectodomain trimeric proteins were prepared as previously
995 described (*83*). Briefly, two human codon-optimized constructs were generated with a human IgG
996 leader sequence, the SARS-CoV-2 spike ectodomain (amino acids 14-1211), a GGSG linker, T4

997 fibritin foldon sequence, a GS linker, and a 15 amino acid biotinylation consensus site (AviTag,
998 construct 1) or 6X-HisTag (construct 2). Each construct was engineered with two sets of mutations
999 to stabilize the protein in a pre-fusion conformation (*83*). Recombinant SARS-CoV-2 spike RBD
1000 domain monomers (human codon-optimized) were generated with a human IgG leader sequence,
1001 the spike RBD (amino acids 319-541 from SARS-CoV-2 Wuhan-Hu-1 strain), a GS linker, an
1002 AviTag, and a 6X-HisTag. The coding sequence of N from SARS-CoV-2 Wuhan-Hu-1 strain was
1003 synthesized in frame with the coding sequence for an AviTag and was cloned in frame to the 6X-
1004 HisTag in the pTrcHis2C expression vector (Invitrogen). Biotinylated recombinant N protein was
1005 produced by co-transforming Rosetta cells with the N expression plasmid and an inducible BirA
1006 expression plasmid. Bacteria were grown in the presence of chloramphenicol, ampicillin, and
1007 streptomycin, induced with IPTG, and supplemented with biotin. Recombinant SARS-CoV-2
1008 Avi/His-tagged spike trimeric proteins were produced by co-transfecting each plasmid construct
1009 (1AVI:2HIS construct ratio) into FreeStyle 293-F cells. The Avi-His-tagged spike RBD protein
1010 was produced by transfecting the single dual-tagged RBD construct into FreeStyle 293-F cells. All
1011 recombinant proteins were purified by FPLC using a nickel-affinity column and subsequent size
1012 exclusion chromatography. After buffer exchange, purified spike ectodomain trimers and RBD
1013 domain protein were biotinylated by the addition of biotin-protein ligase (Avidity). Biotinylated
1014 proteins were buffer exchanged into PBS, sterile filtered, aliquoted, and stored at -80ºC until used.
1015

1016 *SARS-CoV-2 spike cytometric bead array*

1017 CBAs with recombinant SARS-CoV-2 proteins were prepared as previously described (*83*).
1018 Briefly, recombinant proteins were passively absorbed onto streptavidin functionalized 4-µm
1019 fluorescent microparticles (Carboxy Blue Particle Array Kit, Spherotech). 500 µg of biotinylated

1020 recombinant protein was incubated with 2 x 10^7 streptavidin functionalized fluorescent
1021 microparticles in 400 µL of 1% BSA in PBS. Protein coupled beads were washed and resuspended
1022 at 1 x 10^8 beads/mL and stored at 4°C.
1023
1024 *Cytometric bead array measurement of spike-specific IgG responses*
1025 50 µL of serum (diluted to 1/4000 in PBS) or nasal wash (diluted 1/4 in PBS) was arrayed in 96-
1026 well u-bottom polystyrene plates. 5 µL of a suspension containing 5 x 10^5 spike beads, RBD beads,
1027 and N beads was added to the samples. Suspensions were mixed, incubated for 15 minutes at RT,
1028 washed in PBS, stained with FITC-conjugated polyclonal anti-hamster IgG (Southern Biotech) for
1029 15 minutes at RT, washed in PBS, and then resuspended in 100 µL of 1% paraformaldehyde in
1030 PBS. Samples were collected on a BD CytoFLEX flow cytometer in plate mode at a sample rate
1031 of 100 µL/minute for 1 minute. Following acquisition, the FCS files were analyzed in FlowJo
1032 (TreeStar). Briefly, the beads were identified by gating on singlet 4-µm particles in log scale in the
1033 forward scatter and side scatter parameters. APC-Cy7 channel fluorescence gates were used to
1034 segregate the particles by bead identity. Geometric mean fluorescent intensity was calculated in
1035 the FITC channel.
1036
1037 *Propagation and titer determination of SARS-CoV-2*
1038 The original SARS-CoV-2 isolate USA-WA1/2020 was obtained from BEI Resources (#NR-
1039 52281), propagated in Vero E6 cells (ATCC #C1008), and titered as previously described (*84*).
1040

1041 *Viral RNA quantitation by qRT-PCR*

1042 SARS-CoV-2 viral N RNA and viral subgenomic N RNA was measured by PCR in nasal swipe
1043 (300 µL) samples as previously described (*84*). AccuPlex SARS-CoV-2 Reference Material
1044 (SeraCare Life Sciences, Inc., # 0505-0126) was extracted and amplified in parallel to generate a
1045 standard curve enabling viral N quantitation. The subgenomic RNA standard was constructed
1046 and validated in-house (*84*).

1047

1048 *Histopathology*

1049 Hamster lungs were inflated with 10% neutral-buffered formalin (Thermo Fisher) using a blunt
1050 19-gauge needle. Each lung was excised *en bloc* and fixed for 7 days at RT in 15-fold volume of
1051 10% neutral-buffered formalin. The fixed tissues were then embedded dorsal side down in
1052 paraffin using standard procedures. Samples were sectioned at 5 µm, and resulting slides were
1053 stained with hematoxylin and eosin (H&E). All tissue slides were evaluated by light microscopy
1054 by a board-certified veterinary pathologist blinded to study group allocations. Representative
1055 photo images were collected using a Nikon Eclipse Ci microscope (Nikon Inc) and analyzed with
1056 NIS-Elements software (Nikon Inc). Scoring was performed following a published algorithm
1057 (*85*, *86*). Briefly, the airway, alveolar, and vascular pathology in affected areas were assessed
1058 and scored on a scale of 0-4 (*84*), and then added together to generate a total histopathological
1059 score of the whole lung.

1060

1061 *Statistical analysis*

1062 The effect of dosing strategy on CD4 and CD8 cell polyfunctionality was assessed by one-way
1063 ANOVA with Tukey's multiple comparisons test. The effect of dosing strategy on IgG titer and

1064 pseudovirus neutralizing antibody titers was assessed in log-transformed data using a mixed-
1065 effects model with Tukey's multiple comparisons test. The effect of immunization strategy on
1066 IgG titer was assessed on log-transformed data using unpaired *t* tests or two-way ANOVA with
1067 Tukey's or Sidak's (if any sample data were missing) multiple comparisons test. The effect of
1068 immunization strategy on pseudovirus neutralizing antibody titers was assessed on log-
1069 transformed data using unpaired *t* tests or a mixed-effects model with Sidak's multiple
1070 comparisons test. The effect of immunization strategy on polyfunctional CD4 and CD8 cell
1071 responses was assessed in untransformed data using unpaired *t* tests or one-way ANOVA with
1072 Holm-Sidak's multiple comparisons test. Lung, bone marrow, and splenocyte ELISpot data were
1073 analyzed using log-transformed data by one-way ANOVA with Tukey's multiple comparisons
1074 test. Hamster body weight data was analyzed using area under the curve measures assessed
1075 statistically by one-way ANOVA with Tukey's multiple comparison test. Hamster viral load
1076 measures were analyzed using log-transformed area under the curve measures, assessed with
1077 one-way ANOVA with Tukey's multiple comparison test. All statistical analyses were conducted
1078 using Prism version 9 (GraphPad Software).
1079

1080 **References and Notes**

1081 1. V. Mouro, A. Fischer, Dealing with a mucosal viral pandemic: lessons from COVID-19
1082 vaccines. *Mucosal Immunol*, 1–11 (2022).

1083 2. S. M. Kissler, J. R. Fauver, C. Mack, C. G. Tai, M. I. Breban, A. E. Watkins, R. M. Samant,
1084 D. J. Anderson, J. Metti, G. Khullar, R. Baits, M. MacKay, D. Salgado, T. Baker, J. T.
1085 Dudley, C. E. Mason, D. D. Ho, N. D. Grubaugh, Y. H. Grad, Viral dynamics of SARS-

1086 CoV-2 variants in vaccinated and unvaccinated persons. *New England Journal of Medicine*
1087 (2021), doi:10.1056/NEJMc2102507.

1088 3. M. Tiboni, L. Casettari, L. Illum, Nasal vaccination against SARS-CoV-2: synergistic or
1089 alternative to intramuscular vaccines? *Int J Pharm*. **603**, 120686 (2021).

1090 4. M. Garcia-Knight, K. Anglin, M. Tassetto, S. Lu, A. Zhang, S. A. Goldberg, A. Catching,
1091 M. C. Davidson, J. R. Shak, M. Romero, J. Pineda-Ramirez, R. Diaz-Sanchez, P. Rugart, K.
1092 Donohue, J. Massachi, H. M. Sans, M. Djomaleu, S. Mathur, V. Servellita, D. McIlwain, B.
1093 Gaudiliere, J. Chen, E. O. Martinez, J. M. Tavs, G. Bronstone, J. Weiss, J. T. Watson, M.
1094 Briggs-Hagen, G. R. Abedi, G. W. Rutherford, S. G. Deeks, C. Chiu, S. Saydah, M. J.
1095 Peluso, C. M. Midgley, J. N. Martin, R. Andino, J. D. Kelly, Infectious viral shedding of
1096 SARS-CoV-2 Delta following vaccination: A longitudinal cohort study. *PLOS Pathogens*.
1097 **18**, e1010802 (2022).

1098 5. J. Chen, R. Wang, N. B. Gilby, G.-W. Wei, Omicron variant (B.1.1.529): infectivity,
1099 vaccine breakthrough, and antibody resistance. *J. Chem. Inf. Model.* **62**, 412–422 (2022).

1100 6. D. R. Feikin, M. M. Higdon, L. J. Abu-Raddad, N. Andrews, R. Araos, Y. Goldberg, M. J.
1101 Groome, A. Huppert, K. L. O'Brien, P. G. Smith, A. Wilder-Smith, S. Zeger, M. D. Knoll,
1102 M. K. Patel, Duration of effectiveness of vaccines against SARS-CoV-2 infection and
1103 COVID-19 disease: results of a systematic review and meta-regression. *The Lancet*. **399**,
1104 924–944 (2022).

1105 7. R. Link-Gelles, M. E. Levy, M. Gaglani, S. A. Irving, M. Stockwell, K. Dascomb, M. B.
1106 DeSilva, S. E. Reese, I.-C. Liao, T. C. Ong, Effectiveness of 2, 3, and 4 COVID-19 mRNA

1107 vaccine doses among immunocompetent adults during periods when SARS-CoV-2
1108 Omicron BA.1 and BA.2/BA.2.12.1 sublineages predominated — VISION network, 10
1109 states, December 2021–June 2022. *MMWR Morb Mortal Wkly Rep*. **71** (2022),
1110 doi:10.15585/mmwr.mm7129e1.

1111 8. D. Freeman, S. Lambe, L.-M. Yu, J. Freeman, A. Chadwick, C. Vaccari, F. Waite, L.
1112 Rosebrock, A. Petit, S. Vanderslott, S. Lewandowsky, M. Larkin, S. Innocenti, H.
1113 McShane, A. J. Pollard, B. S. Loe, Injection fears and COVID-19 vaccine hesitancy.
1114 *Psychol Med*, 1–11.

1115 9. S. Kar, P. Devnath, T. B. Emran, T. E. Tallei, S. Mitra, K. Dhama, Oral and intranasal
1116 vaccines against SARS-CoV-2: current progress, prospects, advantages, and challenges.
1117 *Immunity, Inflammation and Disease*. **10**, e604 (2022).

1118 10. A. Rice, M. Verma, E. Voigt, P. Battisti, S. Beaver, S. Reed, K. Dinkins, S. Mody, L.
1119 Zakin, S. Tanaka, B. Morimoto, C. A. Olson, E. Gabitzsch, J. T. Safrit, P. Spilman, C.
1120 Casper, P. Soon-Shiong, Heterologous saRNA Prime, DNA Dual-Antigen Boost SARS-
1121 CoV-2 Vaccination Elicits Robust Cellular Immunogenicity and Cross-Variant Neutralizing
1122 Antibodies. *Front Immunol*. **13**, 910136 (2022).

1123 11. E. A. Voigt, A. Gerhardt, D. Hanson, M. F. Jennewein, P. Battisti, S. Reed, J. Singh, R.
1124 Mohamath, J. Bakken, S. Beaver, C. Press, P. Soon-Shiong, C. J. Paddon, C. B. Fox, C.
1125 Casper, A self-amplifying RNA vaccine against COVID-19 with long-term room-
1126 temperature stability. *npj Vaccines*. **7**, 1–13 (2022).

1127 12. Y. Peng, A. J. Mentzer, G. Liu, X. Yao, Z. Yin, D. Dong, W. Dejnirattisai, T. Rostron, P.
1128 Supasa, C. Liu, C. López-Camacho, J. Slon-Campos, Y. Zhao, D. I. Stuart, G. C. Paesen, J.
1129 M. Grimes, A. A. Antson, O. W. Bayfield, D. E. D. P. Hawkins, D.-S. Ker, B. Wang, L.
1130 Turtle, K. Subramaniam, P. Thomson, P. Zhang, C. Dold, J. Ratcliff, P. Simmonds, T. de
1131 Silva, P. Sopp, D. Wellington, U. Rajapaksa, Y.-L. Chen, M. Salio, G. Napolitani, W. Paes,
1132 P. Borrow, B. M. Kessler, J. W. Fry, N. F. Schwabe, M. G. Semple, J. K. Baillie, S. C.
1133 Moore, P. J. M. Openshaw, M. A. Ansari, S. Dunachie, E. Barnes, J. Frater, G. Kerr, P.
1134 Goulder, T. Lockett, R. Levin, Y. Zhang, R. Jing, L.-P. Ho, Oxford Immunology Network
1135 Covid-19 Response T cell Consortium, E. Barnes, D. Dong, T. Dong, S. Dunachie, J.
1136 Frater, P. Goulder, G. Kerr, P. Klenerman, G. Liu, A. McMichael, G. Napolitani, G. Ogg,
1137 Y. Peng, M. Salio, X. Yao, Z. Yin, ISARIC4C Investigators, J. Kenneth Baillie, P.
1138 Klenerman, A. J. Mentzer, S. C. Moore, P. J. M. Openshaw, M. G. Semple, D. I. Stuart, L.
1139 Turtle, R. J. Cornall, C. P. Conlon, P. Klenerman, G. R. Screaton, J. Mongkolsapaya, A.
1140 McMichael, J. C. Knight, G. Ogg, T. Dong, Broad and strong memory CD4+ and CD8+ T
1141 cells induced by SARS-CoV-2 in UK convalescent individuals following COVID-19. *Nat*
1142 *Immunol*. **21**, 1336–1345 (2020).

1143 13. C. Rydyznski Moderbacher, S. I. Ramirez, J. M. Dan, A. Grifoni, K. M. Hastie, D.
1144 Weiskopf, S. Belanger, R. K. Abbott, C. Kim, J. Choi, Y. Kato, E. G. Crotty, C. Kim, S. A.
1145 Rawlings, J. Mateus, L. P. V. Tse, A. Frazier, R. Baric, B. Peters, J. Greenbaum, E.
1146 Ollmann Saphire, D. M. Smith, A. Sette, S. Crotty, Antigen-specific adaptive immunity to
1147 SARS-COV-2 in acute COVID-19 and associations with age and disease severity. *Cell*.
1148 **183**, 996-1012.e19 (2020).

1149 14. Y. Sui, J. Li, H. Andersen, R. Zhang, S. K. Prabhu, T. Hoang, D. Venzon, A. Cook, R.
1150 Brown, E. Teow, J. Velasco, L. Pessaint, I. N. Moore, L. Lagenaur, J. Talton, M. W. Breed,
1151 J. Kramer, K. W. Bock, M. Minai, B. M. Nagata, H. Choo-Wosoba, M. G. Lewis, L.-X.
1152 Wang, J. A. Berzofsky, An intranasally administrated SARS-CoV-2 beta variant subunit
1153 booster vaccine prevents beta variant replication in rhesus macaques. *PNAS Nexus*. **1**,
1154 pgac091 (2022).

1155 15. P. F. McKay, K. Hu, A. K. Blakney, K. Samnuan, J. C. Brown, R. Penn, J. Zhou, C. R.
1156 Bouton, P. Rogers, K. Polra, P. J. C. Lin, C. Barbosa, Y. K. Tam, W. S. Barclay, R. J.
1157 Shattock, Self-amplifying RNA SARS-CoV-2 lipid nanoparticle vaccine candidate induces
1158 high neutralizing antibody titers in mice. *Nat Commun*. **11**, 3523 (2020).

1159 16. R. de Alwis, E. S. Gan, S. Chen, Y. S. Leong, H. C. Tan, S. L. Zhang, C. Yau, J. G. H.
1160 Low, S. Kalimuddin, D. Matsuda, E. C. Allen, P. Hartman, K. J. Park, M. Alayyoubi, H.
1161 Bhaskaran, A. Dukanovic, Y. Bao, B. Clemente, J. Vega, S. Roberts, J. A. Gonzalez, M.
1162 Sablad, R. Yelin, W. Taylor, K. Tachikawa, S. Parker, P. Karmali, J. Davis, B. M. Sullivan,
1163 S. M. Sullivan, S. G. Hughes, P. Chivukula, E. E. Ooi, A single dose of self-transcribing
1164 and replicating RNA-based SARS-CoV-2 vaccine produces protective adaptive immunity
1165 in mice. *Mol Ther*. **29**, 1970–1983 (2021).

1166 17. A. Gerhardt, E. Voigt, M. Archer, S. Reed, E. Larson, N. Van Hoeven, R. Kramer, C. Fox,
1167 C. Casper, A flexible, thermostable nanostructured lipid carrier platform for RNA vaccine
1168 delivery. *Mol Ther Methods Clin Dev*. **25**, 205–214 (2022).

1169 18. H. Xu, L. Cai, S. Hufnagel, Z. Cui, Intranasal vaccine: Factors to consider in research and
1170 development. *Int J Pharm*. **609**, 121180 (2021).

1171 19. L. Feng, Q. Wang, C. Shan, C. Yang, Y. Feng, J. Wu, X. Liu, Y. Zhou, R. Jiang, P. Hu, X.
1172 Liu, F. Zhang, P. Li, X. Niu, Y. Liu, X. Zheng, J. Luo, J. Sun, Y. Gu, B. Liu, Y. Xu, C. Li,
1173 W. Pan, J. Zhao, C. Ke, X. Chen, T. Xu, N. Zhong, S. Guan, Z. Yuan, L. Chen, An
1174 adenovirus-vectored COVID-19 vaccine confers protection from SARS-COV-2 challenge
1175 in rhesus macaques. *Nat Commun*. **11**, 4207 (2020).

1176 20. A. O. Hassan, N. M. Kafai, I. P. Dmitriev, J. M. Fox, B. K. Smith, I. B. Harvey, R. E. Chen,
1177 E. S. Winkler, A. W. Wessel, J. B. Case, E. Kashentseva, B. T. McCune, A. L. Bailey, H.
1178 Zhao, L. A. VanBlargan, Y.-N. Dai, M. Ma, L. J. Adams, S. Shrihari, J. E. Danis, L. E.
1179 Gralinski, Y. J. Hou, A. Schäfer, A. S. Kim, S. P. Keeler, D. Weiskopf, R. S. Baric, M. J.
1180 Holtzman, D. H. Fremont, D. T. Curiel, M. S. Diamond, A single-dose intranasal ChAd
1181 vaccine protects upper and lower respiratory tracts against SARS-CoV-2. *Cell*. **183**, 169-
1182 184.e13 (2020).

1183 21. M.-W. Ku, M. Bourgine, P. Authié, J. Lopez, K. Nemirov, F. Moncoq, A. Noirat, B. Vesin,
1184 F. Nevo, C. Blanc, P. Souque, H. Tabbal, E. Simon, D. Hardy, M. Le Dudal, F. Guinet, L.
1185 Fiette, H. Mouquet, F. Anna, A. Martin, N. Escriou, L. Majlessi, P. Charneau, Intranasal
1186 vaccination with a lentiviral vector protects against SARS-CoV-2 in preclinical animal
1187 models. *Cell Host Microbe*. **29**, 236-249.e6 (2021).

1188 22. N. van Doremalen, J. N. Purushotham, J. E. Schulz, M. G. Holbrook, T. Bushmaker, A.
1189 Carmody, J. R. Port, C. K. Yinda, A. Okumura, G. Saturday, F. Amanat, F. Krammer, P.
1190 W. Hanley, B. J. Smith, J. Lovaglio, S. L. Anzick, K. Barbian, C. Martens, S. C. Gilbert, T.
1191 Lambe, V. J. Munster, Intranasal ChAdOx1 nCoV-19/AZD1222 vaccination reduces viral

1192 shedding after SARS-CoV-2 D614G challenge in preclinical models. *Science Translational*
1193 *Medicine*. **13**, eabh0755 (2021).

1194 23. S. Afkhami, M. R. D'Agostino, A. Zhang, H. D. Stacey, A. Marzok, A. Kang, R. Singh, J.
1195 Bavananthasivam, G. Ye, X. Luo, F. Wang, J. C. Ang, A. Zganiacz, U. Sankar, N.
1196 Kazhdan, J. F. E. Koenig, A. Phelps, S. F. Gameiro, S. Tang, M. Jordana, Y. Wan, K. L.
1197 Mossman, M. Jeyanathan, A. Gillgrass, M. F. C. Medina, F. Smaill, B. D. Lichty, M. S.
1198 Miller, Z. Xing, Respiratory mucosal delivery of next-generation COVID-19 vaccine
1199 provides robust protection against both ancestral and variant strains of SARS-CoV-2. *Cell*.
1200 **185**, 896-915.e19 (2022).

1201 24. M. Cokarić Brdovčak, J. Materljan, M. Šustić, S. Ravlić, T. Ružić, B. Lisnić, K. Miklić, I.
1202 Brizić, M. Pribanić Matešić, V. Juranić Lisnić, B. Halassy, D. Rončević, Z. Knežević, L.
1203 Štefan, F. Bertoglio, M. Schubert, L. Čičin-Šain, A. Markotić, S. Jonjić, A. Krmpotić,
1204 ChAdOx1-S adenoviral vector vaccine applied intranasally elicits superior mucosal
1205 immunity compared to the intramuscular route of vaccination. *European Journal of*
1206 *Immunology*. **52**, 936–945 (2022).

1207 25. H. Lei, A. Alu, J. Yang, W. Ren, C. He, T. Lan, X. He, L. Yang, J. Li, Z. Wang, X. Song,
1208 W. Wang, G. Lu, X. Wei, Intranasal administration of a recombinant RBD vaccine induces
1209 long-term immunity against Omicron-included SARS-CoV-2 variants. *Sig Transduct*
1210 *Target Ther*. **7**, 1–13 (2022).

1211 26. T. Y. Wong, K. S. Lee, B. P. Russ, A. M. Horspool, J. Kang, M. T. Winters, M. Allison
1212 Wolf, N. A. Rader, O. A. Miller, M. Shiflett, J. Izac, D. Varisco, E. Sen-Kilic, C.
1213 Cunningham, M. Cooper, H. A. Cyphert, M. Barbier, I. Martinez, J. R. Bevere, R. K. Ernst,

1214 F. H. Damron, Intranasal administration of BReC-CoV-2 COVID-19 vaccine protects K18-
1215 hACE2 mice against lethal SARS-CoV-2 challenge. *NPJ Vaccines*. **7**, 36 (2022).

1216 27. S. R. Allie, J. E. Bradley, U. Mudunuru, M. D. Schultz, B. A. Graf, F. E. Lund, T. D.
1217 Randall, The establishment of resident memory B cells in the lung requires local antigen
1218 encounter. *Nat Immunol*. **20**, 97–108 (2019).

1219 28. X. An, M. Martinez-Paniagua, A. Rezvan, S. R. Sefat, M. Fathi, S. Singh, S. Biswas, M.
1220 Pourpak, C. Yee, X. Liu, N. Varadarajan, Single-dose intranasal vaccination elicits
1221 systemic and mucosal immunity against SARS-CoV-2. *iScience*. **24**, 103037 (2021).

1222 29. X. F. Li, Z. Cui, H. Fan, Q. Chen, L. Cao, H. Y. Qiu, N. N. Zhang, Y. P. Xu, R. R. Zhang,
1223 C. Zhou, Q. Ye, Y. Q. Deng, Y. Guo, S. Qin, K. Fan, L. Wang, Z. Jia, Y. Cui, X. Wang, C.
1224 F. Qin, A highly immunogenic live-attenuated vaccine candidate prevents SARS-CoV-2
1225 infection and transmission in hamsters. *Innovation (N Y)*, 100221 (2022).

1226 30. A. Ainai, S. Tamura, T. Suzuki, E. van Riet, R. Ito, T. Odagiri, M. Tashiro, T. Kurata, H.
1227 Hasegawa, Intranasal vaccination with an inactivated whole influenza virus vaccine induces
1228 strong antibody responses in serum and nasal mucus of healthy adults. *Hum Vaccin*
1229 *Immunother*. **9**, 1962–70 (2013).

1230 31. K. Dhama, M. Dhawan, R. Tiwari, T. B. Emran, S. Mitra, A. A. Rabaan, S. Alhumaid, Z.
1231 A. Alawi, A. Al Mutair, COVID-19 intranasal vaccines: current progress, advantages,
1232 prospects, and challenges. *Human Vaccines & Immunotherapeutics*, 1–11 (2022).

1233 32. K. McMahan, J. Yu, N. B. Mercado, C. Loos, L. H. Tostanoski, A. Chandrashekar, J. Liu,
1234 L. Peter, C. Atyeo, A. Zhu, E. A. Bondzie, G. Dagotto, M. S. Gebre, C. Jacob-Dolan, Z. Li,

1235 F. Nampanya, S. Patel, L. Pessaint, A. Van Ry, K. Blade, J. Yalley-Ogunro, M. Cabus, R.
1236 Brown, A. Cook, E. Teow, H. Andersen, M. G. Lewis, D. A. Lauffenburger, G. Alter, D. H.
1237 Barouch, Correlates of protection against SARS-CoV-2 in rhesus macaques. *Nature*. **590**,
1238 630–634 (2021).

1239 33. P. B. Gilbert, D. C. Montefiori, A. B. McDermott, Y. Fong, D. Benkeser, W. Deng, H.
1240 Zhou, C. R. Houchens, K. Martins, L. Jayashankar, F. Castellino, B. Flach, B. C. Lin, S.
1241 O'Connell, C. McDanal, A. Eaton, M. Sarzotti-Kelsoe, Y. Lu, C. Yu, B. Borate, L. W. P.
1242 van der Laan, N. S. Hejazi, C. Huynh, J. Miller, H. M. El Sahly, L. R. Baden, M. Baron, L.
1243 De La Cruz, C. Gay, S. Kalams, C. F. Kelley, M. P. Andrasik, J. G. Kublin, L. Corey, K.
1244 M. Neuzil, L. N. Carpp, R. Pajon, D. Follmann, R. O. Donis, R. A. Koup, Immune Assays
1245 Team§, Moderna, Inc. Team§, Coronavirus Vaccine Prevention Network
1246 (CoVPN)/Coronavirus Efficacy (COVE) Team§, United States Government (USG)/CoVPN
1247 Biostatistics Team§, Immune correlates analysis of the mRNA-1273 COVID-19 vaccine
1248 efficacy clinical trial. *Science*. **375**, 43–50 (2022).

1249 34. B. S. Graham, Rapid COVID-19 vaccine development. *Science*. **368**, 945–946 (2020).

1250 35. D. Weiskopf, K. S. Schmitz, M. P. Raadsen, A. Grifoni, N. M. A. Okba, H. Endeman, J. P.
1251 C. van den Akker, R. Molenkamp, M. P. G. Koopmans, E. C. M. van Gorp, B. L.
1252 Haagmans, R. L. de Swart, A. Sette, R. D. de Vries, Phenotype and kinetics of SARS-CoV-
1253 2-specific T cells in COVID-19 patients with acute respiratory distress syndrome. *Sci*
1254 *Immunol*. **5**, eabd2071 (2020).

1255 36. L. A. Jackson, E. J. Anderson, N. G. Rouphael, P. C. Roberts, M. Makhene, R. N. Coler, M.
1256 P. McCullough, J. D. Chappell, M. R. Denison, L. J. Stevens, A. J. Pruijssers, A.

1257 McDermott, B. Flach, N. A. Doria-Rose, K. S. Corbett, K. M. Morabito, S. O'Dell, S. D.
1258 Schmidt, P. A. Swanson, M. Padilla, J. R. Mascola, K. M. Neuzil, H. Bennett, W. Sun, E.
1259 Peters, M. Makowski, J. Albert, K. Cross, W. Buchanan, R. Pikaart-Tautges, J. E.
1260 Ledgerwood, B. S. Graham, J. H. Beigel, R. N. A. S. G. m, An mRNA vaccine against
1261 SARS-CoV-2 - preliminary report. *N Engl J Med*. **383**, 1920–1931 (2020).

1262 37. N. Lurie, M. Saville, R. Hatchett, J. Halton, Developing Covid-19 vaccines at pandemic
1263 speed. *N Engl J Med*. **382**, 1969–1973 (2020).

1264 38. R. Yuan, J. Yu, Z. Jiao, J. Li, F. Wu, R. Yan, X. Huang, C. Chen, The roles of tissue-
1265 resident memory T cells in lung diseases. *Frontiers in Immunology*. **12**, 710375 (2021).

1266 39. R. Elgueta, M. J. Benson, V. C. de Vries, A. Wasiuk, Y. Guo, R. J. Noelle, *Immunol Rev*, in
1267 press, doi:10.1111/j.1600-065X.2009.00782.x.

1268 40. A. Ballesteros-Tato, B. León, F. E. Lund, T. D. Randall, CD4+ T helper cells use CD154–
1269 CD40 interactions to counteract T reg cell–mediated suppression of CD8+ T cell responses
1270 to influenza. *Journal of Experimental Medicine*. **210**, 1591–1601 (2013).

1271 41. J. M. E. Lim, A. T. Tan, N. Le Bert, S. K. Hang, J. G. H. Low, A. Bertoletti, SARS-CoV-2
1272 breakthrough infection in vaccinees induces virus-specific nasal-resident CD8+ and CD4+
1273 T cells of broad specificity. *J Exp Med*. **219**, e20220780 (2022).

1274 42. Y.-J. Park, D. Pinto, A. C. Walls, Z. Liu, A. De Marco, F. Benigni, F. Zatta, C. Silacci-
1275 Fregni, J. Bassi, K. R. Sprouse, A. Addetia, J. E. Bowen, C. Stewart, M. Giurdanella, C.
1276 Saliba, B. Guarino, M. A. Schmid, N. Franko, J. Logue, H. V. Dang, K. Hauser, J. di Iulio,
1277 W. Rivera, G. Schnell, F. A. Lempp, J. Janer, R. Abdelnabi, P. Maes, P. Ferrari, A. Ceschi,

1278 O. Giannini, G. D. de Melo, L. Kergoat, H. Bourhy, J. Neyts, L. Soriaga, L. A. Purcell, G.
1279 Snell, S. P. J. Whelan, A. Lanzavecchia, H. W. Virgin, L. Piccoli, H. Chu, M. S. Pizzuto, D.
1280 Corti, D. Veesler, *bioRxiv*, in press, doi:10.1101/2022.05.08.491108.

1281 43. J. Tang, C. Zeng, T. M. Cox, C. Li, Y. M. Son, I. S. Cheon, Y. Wu, S. Behl, J. J. Taylor, R.
1282 Chakraborty, A. J. Johnson, D. N. Schiavo, J. P. Utz, J. S. Reisenauer, D. E. Midthun, J. J.
1283 Mullon, E. S. Edell, M. G. Alameh, L. Borish, W. G. Teague, M. H. Kaplan, D. Weissman,
1284 R. Kern, H. Hu, R. Vassallo, S.-L. Liu, J. Sun, Respiratory mucosal immunity against
1285 SARS-CoV-2 following mRNA vaccination. *Science Immunology*. **0**, eadd4853 (2022).

1286 44. F. P. Polack, S. J. Thomas, N. Kitchin, J. Absalon, A. Gurtman, S. Lockhart, J. L. Perez, G.
1287 Perez Marc, E. D. Moreira, C. Zerbini, R. Bailey, K. A. Swanson, S. Roychoudhury, K.
1288 Koury, P. Li, W. V. Kalina, D. Cooper, R. W. Frenck, L. L. Hammitt, O. Tureci, H. Nell,
1289 A. Schaefer, S. Unal, D. B. Tresnan, S. Mather, P. R. Dormitzer, U. Sahin, K. U. Jansen,
1290 W. C. Gruber, C. Clinical Trial Group, Safety and efficacy of the BNT162b2 mRNA
1291 Covid-19 vaccine. *N Engl J Med*. **383**, 2603–2615 (2020).

1292 45. L. R. Baden, H. M. El Sahly, B. Essink, K. Kotloff, S. Frey, R. Novak, D. Diemert, S. A.
1293 Spector, N. Rouphael, C. B. Creech, J. McGettigan, S. Khetan, N. Segall, J. Solis, A. Brosz,
1294 C. Fierro, H. Schwartz, K. Neuzil, L. Corey, P. Gilbert, H. Janes, D. Follmann, M.
1295 Marovich, J. Mascola, L. Polakowski, J. Ledgerwood, B. S. Graham, H. Bennett, R. Pajon,
1296 C. Knightly, B. Leav, W. Deng, H. Zhou, S. Han, M. Ivarsson, J. Miller, T. Zaks, Cove
1297 Study Group, Efficacy and safety of the mRNA-1273 SARS-CoV-2 vaccine. *N Engl J Med*.
1298 **384**, 403–416 (2021).

1299 46. H. M. El Sahly, L. R. Baden, B. Essink, S. Doblecki-Lewis, J. M. Martin, E. J. Anderson,
1300 T. B. Campbell, J. Clark, L. A. Jackson, C. J. Fichtenbaum, M. Zervos, B. Rankin, F. Eder,
1301 G. Feldman, C. Kennelly, L. Han-Conrad, M. Levin, K. M. Neuzil, L. Corey, P. Gilbert, H.
1302 Janes, D. Follmann, M. Marovich, L. Polakowski, J. R. Mascola, J. E. Ledgerwood, B. S.
1303 Graham, A. August, H. Clouting, W. Deng, S. Han, B. Leav, D. Manzo, R. Pajon, F.
1304 Schodel, J. E. Tomassini, H. Zhou, J. Miller, Cove Study Group, Efficacy of the mRNA-
1305 1273 SARS-CoV-2 vaccine at completion of blinded phase. *N Engl J Med*. **385**, 1774–1785
1306 (2021).

1307 47. O. J. Watson, G. Barnsley, J. Toor, A. B. Hogan, P. Winskill, A. C. Ghani, Global impact
1308 of the first year of COVID-19 vaccination: a mathematical modelling study. *The Lancet*
1309 *Infectious Diseases*. **0** (2022), doi:10.1016/S1473-3099(22)00320-6.

1310 48. G. Giannotta, N. Giannotta, mRNA COVID-19 vaccines and long-lived plasma cells: a
1311 complicated relationship. *Vaccines (Basel)*. **9**, 1503 (2021).

1312 49. F. J. Ibarrondo, C. Hofmann, J. A. Fulcher, D. Goodman-Meza, W. Mu, M. A. Hausner, A.
1313 Ali, A. Balamurugan, E. Taus, J. Elliott, P. Krogstad, N. H. Tobin, K. G. Ferbas, S. G.
1314 Kitchen, G. M. Aldrovandi, A. W. Rimoin, O. O. Yang, Primary, recall, and decay kinetics
1315 of SARS-CoV-2 vaccine antibody responses. *ACS Nano*. **15**, 11180–11191 (2021).

1316 50. J. Keehner, L. E. Horton, N. J. Binkin, L. C. Laurent, D. Pride, C. A. Longhurst, S. R.
1317 Abeles, F. J. Torriani, Resurgence of SARS-CoV-2 infection in a highly vaccinated health
1318 system workforce. *N Engl J Med*. **385**, 1330–1332 (2021).

1319 51. C. Menni, A. May, L. Polidori, P. Louca, J. Wolf, J. Capdevila, C. Hu, S. Ourselin, C. J.
1320 Steves, A. M. Valdes, T. D. Spector, COVID-19 vaccine waning and effectiveness and
1321 side-effects of boosters: a prospective community study from the ZOE COVID Study. *The*
1322 *Lancet Infectious Diseases*. **22**, 1002–1010 (2022).

1323 52. S. Rele, COVID-19 vaccine development during pandemic: gap analysis, opportunities, and
1324 impact on future emerging infectious disease development strategies. *Hum Vaccin*
1325 *Immunother*. **17**, 1122–1127 (2021).

1326 53. X. Ren, J. Zhou, J. Guo, C. Hao, M. Zheng, R. Zhang, Q. Huang, X. Yao, R. Li, Y. Jin,
1327 Reinfection in patients with COVID-19: a systematic review. *Glob Health Res Policy*. **7**, 12
1328 (2022).

1329 54. Y. Araf, F. Akter, Y.-D. Tang, R. Fatemi, M. S. A. Parvez, C. Zheng, M. G. Hossain,
1330 Omicron variant of SARS-CoV-2: Genomics, transmissibility, and responses to current
1331 COVID-19 vaccines. *J Med Virol*. **94**, 1825–1832 (2022).

1332 55. D. W. Eyre, D. Taylor, M. Purver, D. Chapman, T. Fowler, K. B. Pouwels, A. S. Walker, T.
1333 E. A. Peto, Effect of Covid-19 Vaccination on Transmission of Alpha and Delta Variants.
1334 *New England Journal of Medicine*. **386**, 744–756 (2022).

1335 56. C. Franco-Paredes, Transmissibility of SARS-CoV-2 among fully vaccinated individuals.
1336 *The Lancet Infectious Diseases*. **22**, 16 (2022).

1337 57. A. Singanayagam, S. Hakki, J. Dunning, K. J. Madon, M. A. Crone, A. Koycheva, N.
1338 Derqui-Fernandez, J. L. Barnett, M. G. Whitfield, R. Varro, A. Charlett, R. Kundu, J. Fenn,
1339 J. Cutajar, V. Quinn, E. Conibear, W. Barclay, P. S. Freemont, G. P. Taylor, S. Ahmad, M.

1340 Zambon, N. M. Ferguson, A. Lalvani, A. Badhan, S. Dustan, C. Tejpal, A. V. Ketkar, J. S.
1341 Narean, S. Hammett, E. McDermott, T. Pillay, H. Houston, C. Luca, J. Samuel, S.
1342 Bremang, S. Evetts, J. Poh, C. Anderson, D. Jackson, S. Miah, J. Ellis, A. Lackenby,
1343 Community transmission and viral load kinetics of the SARS-CoV-2 delta (B.1.617.2)
1344 variant in vaccinated and unvaccinated individuals in the UK: a prospective, longitudinal,
1345 cohort study. *The Lancet Infectious Diseases*. **22**, 183–195 (2022).

1346 58. M. Cevik, N. D. Grubaugh, A. Iwasaki, P. Openshaw, COVID-19 vaccines: Keeping pace
1347 with SARS-CoV-2 variants. *Cell*. **184**, 5077–5081 (2021).

1348 59. M. C. Maher, I. Bartha, S. Weaver, J. di Iulio, E. Ferri, L. Soriaga, F. A. Lempp, B. L. Hie,
1349 B. Bryson, B. Berger, D. L. Robertson, G. Snell, D. Corti, H. W. Virgin, S. L. Kosakovsky
1350 Pond, A. Telenti, Predicting the mutational drivers of future SARS-CoV-2 variants of
1351 concern. *Science Translational Medicine*. **14**, eabk3445 (2022).

1352 60. C. Zhong, H. Xia, A. Adam, B. Wang, R. L. Hajnik, Y. Liang, G. H. Rafael, J. Zou, X.
1353 Wang, J. Sun, L. Soong, A. D. T. Barrett, S. C. Weaver, P.-Y. Shi, T. Wang, H. Hu,
1354 Mucosal vaccination induces protection against SARS-CoV-2 in the absence of detectable
1355 neutralizing antibodies. *NPJ Vaccines*. **6**, 139 (2021).

1356 61. P. F. Wright, A. C. Prevost-Reilly, H. Natarajan, E. B. Brickley, R. I. Connor, W. F.
1357 Wieland-Alter, A. S. Miele, J. A. Weiner, R. D. Nerenz, M. E. Ackerman, Longitudinal
1358 Systemic and Mucosal Immune Responses to SARS-CoV-2 Infection. *The Journal of*
1359 *Infectious Diseases*, jiac065 (2022).

1360 62. A. Alu, L. Chen, H. Lei, Y. Wei, X. Tian, X. Wei, Intranasal COVID-19 vaccines: From
1361 bench to bed. *eBioMedicine*. **76** (2022), doi:10.1016/j.ebiom.2022.103841.

1362 63. H. E. Mudrick, E. B. McGlinch, B. J. Parrett, J. R. Hemsath, M. E. Barry, J. D. Rubin, C.
1363 Uzendu, M. J. Hansen, C. L. Erskine, V. P. VanKeulen, A. Drelich, C.-T. K. Tseng, S.
1364 Massey, M. Fida, G. A. Suh, T. Peikert, M. S. Block, G. R. Olivier, M. A. Barry,
1365 Comparison of Mucosal and Intramuscular Immunization against SARS-CoV-2 with
1366 Replication-Defective and Replicating Single-cycle Adenovirus Vaccines (2021), p.
1367 2021.04.20.440651, , doi:10.1101/2021.04.20.440651.

1368 64. N. J. Carter, M. P. Curran, Live attenuated influenza vaccine (FluMist®; Fluenz™): a
1369 review of its use in the prevention of seasonal influenza in children and adults. *Drugs*. **71**,
1370 1591–1622 (2011).

1371 65. S. R. Banihashemi, A. Es-haghi, M. H. Fallah Mehrabadi, M. Nofeli, A. R. Mokarram, A.
1372 Ranjbar, M. Salman, M. Hajimoradi, S. H. Razaz, M. Taghdiri, M. Bagheri, M. Dadar, Z.
1373 M. Hassan, M. Eslampanah, Z. Salehi Najafabadi, M. Lotfi, A. Khorasani, F. Rahmani,
1374 Safety and Efficacy of Combined Intramuscular/Intranasal RAZI-COV PARS Vaccine
1375 Candidate Against SARS-CoV-2: A Preclinical Study in Several Animal Models. *Front*
1376 *Immunol*. **13**, 836745 (2022).

1377 66. E. Waltz, China and India approve nasal COVID vaccines — are they a game changer?
1378 *Nature*. **609**, 450–450 (2022).

1379 67. F. Xu, S. Wu, L. Yi, S. Peng, F. Wang, W. Si, L. Hou, T. Zhu, Safety, mucosal and
1380 systemic immunopotency of an aerosolized adenovirus-vectored vaccine against SARS-
1381 CoV-2 in rhesus macaques. *Emerging Microbes & Infections*. **11**, 439–442 (2022).

1382 68. B. Slütter, L. L. Pewe, S. M. Kaech, J. T. Harty, Lung Airway-Surveilling CXCR3hi
1383 Memory CD8+ T Cells Are Critical for Protection against Influenza A Virus. *Immunity*. **39**,
1384 939–948 (2013).

1385 69. A. Rice, M. Verma, A. Shin, L. Zakin, P. Sieling, S. Tanaka, J. Balint, K. Dinkins, H.
1386 Adisetiyo, B. Morimoto, W. Higashide, C. Anders Olson, S. Mody, P. Spilman, E.
1387 Gabitzsch, J. T. Safrit, S. Rabizadeh, K. Niazi, P. Soon-Shiong, Intranasal plus
1388 subcutaneous prime vaccination with a dual antigen COVID-19 vaccine elicits T-cell and
1389 antibody responses in mice. *Sci Rep*. **11**, 14917 (2021).

1390 70. T. Y. Wong, K. S. Lee, B. P. Russ, A. M. Horspool, J. Kang, M. T. Winters, M. Allison
1391 Wolf, N. A. Rader, O. A. Miller, M. Shiflett, J. Izac, D. Varisco, E. Sen-Kilic, C.
1392 Cunningham, M. Cooper, H. A. Cyphert, M. Barbier, I. Martinez, J. R. Bevere, R. K. Ernst,
1393 F. H. Damron, Intranasal administration of BReC-CoV-2 COVID-19 vaccine protects K18-
1394 hACE2 mice against lethal SARS-CoV-2 challenge. *NPJ Vaccines*. **7**, 36 (2022).

1395 71. K. S. Corbett, D. K. Edwards, S. R. Leist, O. M. Abiona, S. Boyoglu-Barnum, R. A.
1396 Gillespie, S. Himansu, A. Schäfer, C. T. Ziwawo, A. T. DiPiazza, K. H. Dinnon, S. M.
1397 Elbashir, C. A. Shaw, A. Woods, E. J. Fritch, D. R. Martinez, K. W. Bock, M. Minai, B. M.
1398 Nagata, G. B. Hutchinson, K. Wu, C. Henry, K. Bahl, D. Garcia-Dominguez, L. Ma, I.
1399 Renzi, W.-P. Kong, S. D. Schmidt, L. Wang, Y. Zhang, E. Phung, L. A. Chang, R. J.
1400 Loomis, N. E. Altaras, E. Narayanan, M. Metkar, V. Presnyak, C. Liu, M. K. Louder, W.

1401 Shi, K. Leung, E. S. Yang, A. West, K. L. Gully, L. J. Stevens, N. Wang, D. Wrapp, N. A.
1402 Doria-Rose, G. Stewart-Jones, H. Bennett, G. S. Alvarado, M. C. Nason, T. J. Ruckwardt,
1403 J. S. McLellan, M. R. Denison, J. D. Chappell, I. N. Moore, K. M. Morabito, J. R. Mascola,
1404 R. S. Baric, A. Carfi, B. S. Graham, SARS-CoV-2 mRNA vaccine design enabled by
1405 prototype pathogen preparedness. *Nature*. **586**, 567–571 (2020).

1406 72. P. Naaber, L. Tserel, K. Kangro, E. Sepp, V. Jürjenson, A. Adamson, L. Haljasmägi, A. P.
1407 Rumm, R. Maruste, J. Kärner, J. M. Gerhold, A. Planken, M. Ustav, K. Kisand, P. Peterson,
1408 Dynamics of antibody response to BNT162b2 vaccine after six months: a longitudinal
1409 prospective study. *The Lancet Regional Health - Europe*. **10**, 100208 (2021).

1410 73. J. L. Americo, C. A. Cotter, P. L. Earl, R. Liu, B. Moss, Intranasal inoculation of an MVA-
1411 based vaccine induces IgA and protects the respiratory tract of hACE2 mice from SARS-
1412 CoV-2 infection. *Proc Natl Acad Sci U S A*. **119**, e2202069119 (2022).

1413 74. J. R. Francica, B. J. Flynn, K. E. Foulds, A. T. Noe, A. P. Werner, I. N. Moore, M. Gagne,
1414 T. S. Johnston, C. Tucker, R. L. Davis, B. Flach, S. O'Connell, S. F. Andrew, E. Lamb, D.
1415 R. Flebbe, S. T. Nurmukhambetova, M. M. Donaldson, J.-P. M. Todd, A. L. Zhu, C. Atyeo,
1416 S. Fischinger, M. J. Gorman, S. Shin, V. V. Edara, K. Floyd, L. Lai, S. Boyoglu-Barnum,
1417 R. Van De Wetering, A. Tylor, E. McCarthy, V. Lecouturier, S. Ruiz, C. Berry, T. Tibbitts,
1418 H. Andersen, A. Cook, A. Dodson, L. Pessaint, A. Van Ry, M. Koutsoukos, C. Gutzeit, I.-
1419 T. Teng, T. Zhou, D. Li, B. F. Haynes, P. D. Kwong, A. McDermott, M. G. Lewis, T. M.
1420 Fu, R. Chicz, R. van der Most, K. S. Corbett, M. S. Suthar, G. Alter, M. Roederer, N. J.
1421 Sullivan, D. C. Douek, B. S. Graham, D. Casimiro, R. A. Seder, Protective antibodies

1422 elicited by SARS-CoV-2 spike protein vaccination are boosted in the lung after challenge in
1423 nonhuman primates. *Science Translational Medicine*. **13**, eabi4547 (2021).

1424 75. T. Mao, B. Israelow, A. Suberi, L. Zhou, M. Reschke, M. A. Peña-Hernández, H. Dong, R.
1425 J. Homer, W. M. Saltzman, A. Iwasaki, *bioRxiv*, in press, doi:10.1101/2022.01.24.477597.

1426 76. ImmunityBio, Inc., "THEMBA II T-CELL Vaccine: A Phase 1/2 Study of the Safety,
1427 Reactogenicity, and Immunogenicity of Vaccination With saRNA COVID-19 Vaccines"
1428 (Clinical trial registration NCT05370040, clinicaltrials.gov, 2022), (available at
1429 https://clinicaltrials.gov/ct2/show/NCT05370040).

1430 77. J. Grimaud, V. N. Murthy, How to monitor breathing in laboratory rodents: a review of the
1431 current methods. *Journal of Neurophysiology*. **120**, 624–632 (2018).

1432 78. Y. M. Son, I. S. Cheon, Y. Wu, C. Li, Z. Wang, X. Gao, Y. Chen, Y. Takahashi, Y.-X. Fu,
1433 A. L. Dent, M. H. Kaplan, J. J. Taylor, W. Cui, J. Sun, Tissue-resident CD4+ T helper cells
1434 assist the development of protective respiratory B and CD8+ T cell memory responses. *Sci*
1435 *Immunol*. **6**, eabb6852 (2021).

1436 79. N. Swarnalekha, D. Schreiner, L. C. Litzler, S. Iftikhar, D. Kirchmeier, M. Künzli, Y. M.
1437 Son, J. Sun, E. A. Moreira, C. G. King, T resident helper cells promote humoral responses
1438 in the lung. *Sci Immunol*. **6**, eabb6808 (2021).

1439 80. J. H. Erasmus, A. P. Khandhar, J. Guderian, B. Granger, J. Archer, M. Archer, E. Gage, J.
1440 Fuerte-Stone, E. Larson, S. Lin, R. Kramer, R. N. Coler, C. B. Fox, D. T. Stinchcomb, S. G.
1441 Reed, N. Van Hoeven, A Nanostructured Lipid Carrier for Delivery of a Replicating Viral
1442 RNA Provides Single, Low-Dose Protection against Zika. *Mol Ther*. **26**, 2507–2522 (2018).

1443 81. Committee for the Update of the Guide for the Care and Use of Laboratory Animals, *Guide*
1444 *for the Care and Use of Laboratory Animals* (The National Academies Press, Washington,
1445 DC, USA, Eighth., 2011).

1446 82. K. H. D. Crawford, R. Eguia, A. S. Dingens, A. N. Loes, K. D. Malone, C. R. Wolf, H. Y.
1447 Chu, M. A. Tortorici, D. Veesler, M. Murphy, D. Pettie, N. P. King, A. B. Balazs, J. D.
1448 Bloom, Protocol and reagents for pseudotyping lentiviral particles with SARS-CoV-2 spike
1449 protein for neutralization assays. *Viruses*. **12**, 513 (2020).

1450 83. R. G. King, A. Silva-Sanchez, J. N. Peel, D. Botta, A. M. Dickson, A. K. Pinto, S. Meza-
1451 Perez, S. R. Allie, M. D. Schultz, M. Liu, J. E. Bradley, S. Qiu, G. Yang, F. Zhou, E.
1452 Zumaquero, T. S. Simpler, B. Mousseau, J. T. Killian, B. Dean, Q. Shang, J. L. Tipper, C.
1453 A. Risley, K. S. Harrod, T. Feng, Y. Lee, B. Shiberu, V. Krishnan, I. Peguillet, J. Zhang, T.
1454 J. Green, T. D. Randall, J. J. Suschak, B. Georges, J. D. Brien, F. E. Lund, M. S. Roberts,
1455 Single-Dose Intranasal Administration of AdCOVID Elicits Systemic and Mucosal
1456 Immunity against SARS-CoV-2 and Fully Protects Mice from Lethal Challenge. *Vaccines*
1457 *(Basel)*. **9**, 881 (2021).

1458 84. M. D. Schultz, J. J. Suschak, D. Botta, A. Silva-Sanchez, R. G. King, T. W. Detchemendy,
1459 C. D. Meshram, J. B. Foote, F. Zhou, J. L. Tipper, J. Zhang, K. S. Harrod, S. M. Leal, T. D.
1460 Randall, M. S. Roberts, B. Georges, F. E. Lund, A single intranasal administration of
1461 AdCOVID protects against SARS-CoV-2 infection in the upper and lower respiratory
1462 tracts. *Human Vaccines & Immunotherapeutics*. **0**, 2127292 (2022).

1463 85. T. Carroll, D. Fox, N. van Doremalen, E. Ball, M. K. Morris, A. Sotomayor-Gonzalez, V.
1464 Servellita, A. Rustagi, C. K. Yinda, L. Fritts, J. R. Port, Z.-M. Ma, M. G. Holbrook, J.

1465 Schulz, C. A. Blish, C. Hanson, C. Y. Chiu, V. Munster, S. Stanley, C. J. Miller, The
1466 B.1.427/1.429 (epsilon) SARS-CoV-2 variants are more virulent than ancestral B.1 (614G)
1467 in Syrian hamsters. *PLOS Pathogens*. **18**, e1009914 (2022).

1468 86. A. D. Gruber, N. Osterrieder, L. D. Bertzbach, D. Vladimirova, S. Greuel, J. Ihlow, D.
1469 Horst, J. Trimpert, K. Dietert, Standardization of Reporting Criteria for Lung Pathology in
1470 SARS-CoV-2-infected Hamsters: What Matters? *Am J Respir Cell Mol Biol*. **63**, 856–859
1471 (2020).

1472

1473 **Acknowledgments:**
1474 We thank Jesse Bloom (Fred Hutchinson Cancer Center) for sharing the SARS-CoV-2 spike
1475 protein plasmids used in pseudovirus production. We are additionally grateful to Robert Kinsey,
1476 who conducted the manufacture of the NLC used in these studies; Christopher Press, who
1477 manufactured some RNA products used in this study; Jeff Guderian; and Ethan Lo. We also
1478 thank Theresa Britschgi, who was instrumental as project manager for this work, and Valerie
1479 Soza, for editorial assistance. We also gratefully acknowledge Thomas 'Scott' Simpler and
1480 Rebecca Burnham for ABSL2 hamster husbandry, Donovan J. Murphy for ABSL3 hamster
1481 husbandry, Jennifer L. Tipper and Kevin Harrod (UAB Department of Anesthesiology and
1482 Perioperative Medicine) for providing SARS-CoV-2 viral stock, Levi Schaefers and Sixto M.
1483 Leal Jr. (UAB Fungal Reference Lab) for viral RNA quantitation, and Emily E. Helmen and
1484 Sherri Coffman (UAB Comparative Pathology Lab) for histology.

1485

Funding:

This work was funded in part by sponsored research from ImmunityBio, Inc. Development and validation of the CBA array was supported by NIH U19 AI142737. The UAB SEBLAB was supported by NIAID Regional Biocontainment Lab (RBL) awards UC6AI058599, 1G20AI167409-01, and 1G20AI167409-S1. The content is solely the responsibility of the authors and does not necessarily represent the views of the funders.

Author Contributions

Conceptualization: MFJ, EAV, FEL

Supervision: MFJ, EAV, AG, TDR, FEL

Project administration: MFJ, EAV, AG, DB, FEL

Funding acquisition: EAV, CC, FEL

Investigation: MFJ, SB, DH, PB, JB, DH, RM, JS, NC, SR, MDS, DB, AS-S, DK, JA, GRK

Data curation: MFJ

Formal analysis: MFJ, SB, PB, NC, EAV, MDS

Writing – original draft: MFJ, EAV

Writing – review & editing: all authors

Competing Interests

AG and EAV declare no Competing Non-Financial Interests but the following Competing Financial Interests. AG and EAV are co-inventors on PCT patent application PCT/US21/40388, "Co-lyophilized RNA and Nanostructured Lipid Carrier," and related national filings, as well as U.S provisional patent application 63/345,345, "Intranasal Administration of Thermostable RNA

1509 Vaccines," and 63/144,169, "A thermostable, flexible RNA vaccine delivery platform for
1510 pandemic response." All other authors declare that they have no competing interests.
1511
1512 **Data and Materials Availability**
1513 The datasets generated and/or analyzed during the current study are available from the
1514 corresponding author on reasonable request. AAHI's unique saRNA constructs and nanostructured
1515 lipid carriers are available for noncommercial research, academic non-clinical research, or other
1516 not-for-profit scholarly purposes undertaken at a non-profit or government institution, under the
1517 terms and conditions of an appropriate Material Transfer Agreement. Correspondence and material
1518 requests should be addressed to the corresponding author.
1519
1520 **Supplementary Materials:**
1521 Figure S1. Spleen flow cytometry gating strategy.
1522 Figure S2. Th1-Th2 balance of SARS-CoV-2 spike-responsive $CD4^+$ cells after prime-boost
1523 immunization with SARS-CoV-2 saRNA-NLC vaccine.
1524 Figure S3. Lung flow cytometry gating strategy.
1525 Figure S4. Vaccine antibody responses in naive cagemates of sham-vaccinated and vaccinated
1526 hamsters.
1527 Figure S5. Correlation between body weight and serum anti-spike IgG titer in mice vaccinated
1528 with SARS-CoV-2 saRNA-NLC vaccine and experimentally infected with SARS-CoV-2.
1529 Figure S6. Vaccination with SARS-CoV-2 saRNA-NLC vaccine reduces lung pathology in both
1530 vaccinated hamsters and naive cagemates irrespective of route of priming and boosting
1531 immunization.